AN ABSTRACT OF THE THESIS OF

Meisam Shir Mohammadi for the degree of Master of Science in Materials Science presented on June 14, 2012

Title: Fracture Properties of Balsa Wood and Balsa Core Sandwich Composites

Abstract approved:

John A. Nairn

Favorable properties of Balsa wood make it an interesting alternative in a number of applications including thermal insulation or as a lightweight core material in sandwich composites. Increasing use in construction necessitates a better understanding of its mechanical and failure properties. In the present work, mode I and mode II fracture toughness for different types of balsa wood and a sandwich structure (balsa as core and fiber glass as skin layer) are studied experimentally by using load-displacement diagrams and visually acquired crack growth data.

# Fracture Properties of Balsa Wood and Balsa Core Sandwich Composites

By:

Meisam Shir Mohammadi

A THESIS

Submitted to

Oregon State University

In partial fulfillment of

the requirements for the

degree of

Master of Science

Presented June 14, 2012

Commencement June 2013

Master of Science thesis of Meisam Shir Mohammadi presented on June 14, 2012.

APPROVED:

_____

Major Professor, representing Materials Science

_____

Director of the Materials Science Graduate Program

_____

Dean of the Graduate School

I understand that my thesis will become part of the permanent collection of Oregon State University libraries. My signature below authorizes release of my thesis to any reader upon request.

_____

Meisam Shir Mohammadi, Author

TABLE OF CONTENTS

TABLE OF CONTENTS

LIST OF FIGURES

Figure Page

LIST OF FIGURES (CONTINUED)

Figure Page

LIST OF FIGURES (CONTINUED)

Figure Page

LIST OF FIGURES (CONTINUED)

Figure Page

# LIST OF TABLES

Table Page

# Chapter 1. Introduction

## *1.1. History of Balsa wood*

Balsa *(Ochroma which means in Greek lingo paleness*) belongs to the corkwood family. It is mostly found in tropical areas in South America [1]. It is usually found at lower elevations from sea level to 3000 feet (1000m), preferring bottomland soil close to streams and rivers [1]. Balsa in Spanish means raft and it has history among the Polynesian peoples. Around 500 A.D Peruvians used Balsa trees to construct their Kon-Tiki rafts [2]. Nowadays, Ecuador is the largest provider of commercial balsa wood where it was originally called Boya, meaning buoy [1]. Several characteristic of balsa give in many possible uses. It is the softest and the lightest commercial wood. Its density is low and varies over a wide range (from 40 to 320 kg/m$^3$) depending on age and habitat of trees. The botanists know eleven species of this wood [2]. The average density of these woods, which are selected for use in United States, is around 180 kg m$^{-3}$ (11 lb ft$^{-3}$) when dry and often as low as 100 kg m$^{-3}$ (6 lb ft$^{-3}$). This wood can be easily recognized by its lightweight, color (oatmeal color, yellowish, or pinkish hue) and unique velvety looks [1]. This tree grows rapidly, especially during its few years of life. It is common for them to attain 70 feet (21.5 m) height and 1.5-2 feet (40-60 cm) diameter in 7 years. The leaves on young tree are very large. Some have length of 40 inches and for mature trees the length varies from 10 to 15 inches. Lumbermen prefer to log Balsa trees when they are 6-7 years old because after that it becomes hard and heavy [2].

In the United States, Balsa was used for aircraft in the early 1920s. It was also widely used for construction of grinders and as a part of the skin of the World War II Mosquito fighter plane [1]. Balsa is highly efficient in uses where buoyancy, insulation against heat (or cold) or low propagation of sound and vibration are important, because of its lightweight and porous composition. Today, it is mainly used for thermal insulation of refrigerated ships, for floating in lifeboats, as a

lightweight core material in composite sandwich boards, for packaging and for making models [1].

*1.2. Structure of Balsa wood*

Much of the volume of Balsa wood is made up of hexagonal-prismatic cells, with aspect ratio of about 16:1, occasionally subdivided by transverse walls. These large cells are partitioned by rays that are smaller and have a different shape [1]. This structure is penetrated by sap channels running parallel to the axis of the tree. Growth rings are perpendicular to the rays. Figure 1.1 shows a micrograph of balsa and figure 1.2 has a diagram of the structure [1].

Mechanical tests have been done on balsa wood but none of them addressed fracture toughness of balsa wood. Esterling investigated compressive stress-strain curves for medium density balsa wood, 0.127-0.160 gr/cm$^3$, in tangential, radial and longitudinal directions and compared structure changes during deformation. Figure 1.3 shows these compression stress-strain curves in different directions [1]. They reported the basic mechanical properties of balsa wood for four different densities (Table 1). Furthermore, Dreisbach (1951), reported mechanical properties of balsa wood, fracture toughness is included, but it did not address methods for finding the toughness and the result seems to be inaccurate [2].

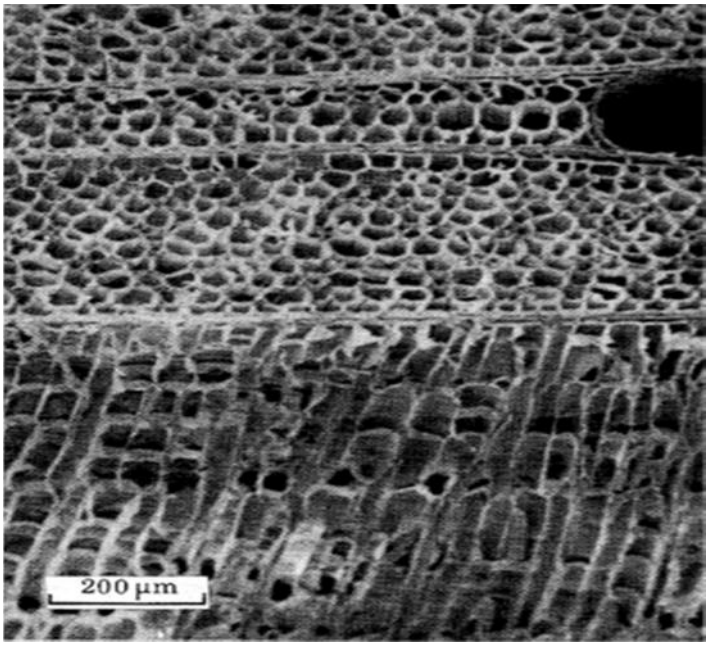


Figure 1.1. Microscopic picture of Balsa showing axial (top) and tangential (bottom) faces, rays (horizontal bands) and sap channels [1].

Table 1.1. Measured and calculated properties of for different densities of Balsa wood [1].

| specimen ... | | S | | M1 | | M2 | | H | |
|---|---|---|---|---|---|---|---|---|---|
| property | eqn | expt | theory | expt | theory | expt | theory | expt | theory |
| $\rho/(kg/m^3)$ | — | 78 | — | 127 | — | 160 | — | 218 | — |
| $E_T/(MN/m^2)$ | (3) | 13 | 2.1 | 32 | 9.1 | 39 | 18.2 | 59 | 46 |
| $E_R/(MN/m^2)$ | (4) | 53 | 4.2 | 67 | 18.2 | 86 | 36.4 | 172 | 92 |
| $E_A/(MN/m^2)$ | (5) | 903 | 1820 | 2870 | 2960 | 3330 | 3730 | 5900 | 5090 |
| $\sigma_T^*/(MN/m^2)$ | (6) | 0.3 | 0.36 | 0.69 | 0.98 | 0.81 | 1.5 | 1.6 | 2.8 |
| $\sigma_R^*/MN/m^2)$ | (7) | 0.66 | 0.5 | 0.94 | 1.4 | 1.0 | 2.2 | 2.1 | 4.0 |
| $\sigma_A^*(MN/m^2)$ | (8) | 4.6 | 6.0 | 8.5 | 10.0 | 12.0 | 12.6 | 17.2 | 17.0 |
| $\nu_{TA}$ | — | — | — | 0.011 | 0 | — | — | — | — |
| $\nu_{TR}$ | — | — | — | 0.034 | 1 | — | — | — | — |
| $\nu_{RA}$ | — | — | — | 0.014 | 0 | — | — | — | — |
| $\nu_{RT}$ | — | — | — | 0.65 | 1 | — | — | — | — |

*1.3. Wood directions:*

There are three orthogonal planes for woods: Radial (R), Tangential (T) and axial or longitudinal (L). If wood is cut at sufficient distance from the tree's center, curvature of growth rings can be minimized such that the orthogonal axes of the board can be approximated as being along R, T, and L directions. In wood, six systems of crack propagation can be defined – LR, LT, TL, RL, RT, and TR. The first letter indicates the normal to the crack plane and the second letter describes the direction of crack propagation. In practice, cracks never propagate in the LR or LT direction because

that would require fracture of wood fibers. Instead, cracks oriented in those direction turn to become RL, TL, RT, or TR fracture. Figure 1.4 shows all of these directions along wood growth axis [3].

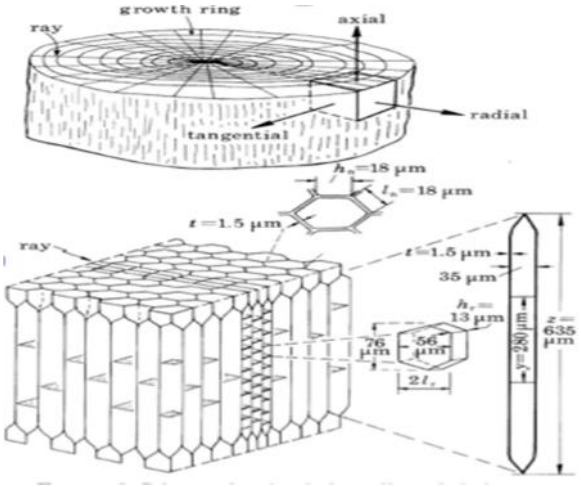


Figure 1.2. Schematic picture of Balsa cells [1].

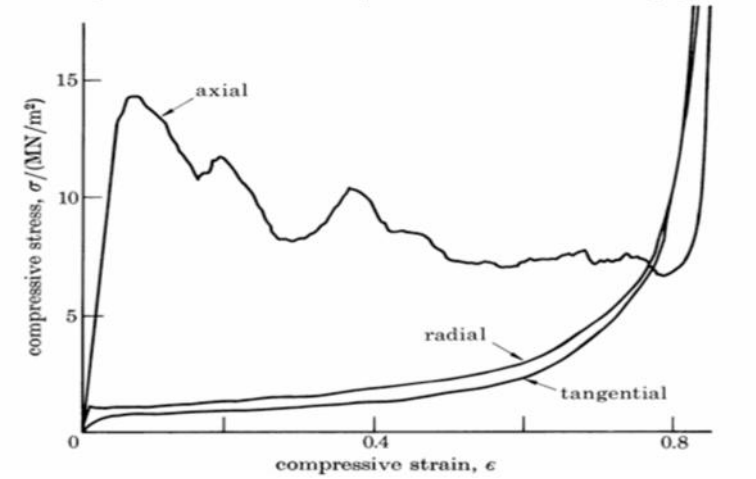


Figure 1.3. Stress-strain curve for midum density Balsa wood [1].

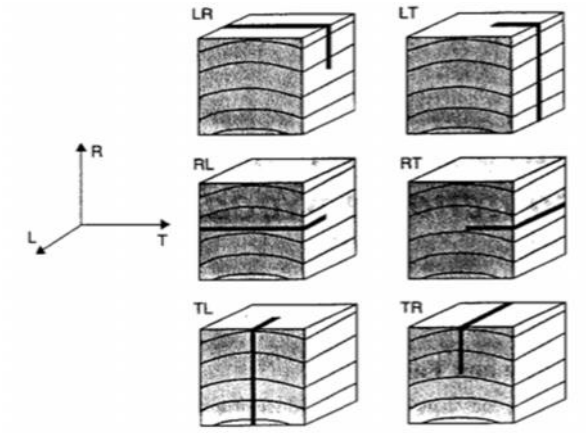


Figure 1.4. Different directions in wood samples in wood growth direction [3].

*1.4. Different types of fracture (Mode I, Mode II, Mixed mode):*

For wood materials mode I tensile cracking is the most critical fracture that could be induced by any arbitrary stress. The mode I fracture parallel to the grain is more interesting for wood industry because usually the strengths in radial or tangential directions are only 10-30% of longitudinal direction. Mode I is the type of fracture in which crack propagates perpendicular to stress direction [3].

Stress intensify factor ($K_I$) characterizes crack-tip stress state and it is a function of crack length ($a$), the applied stress ($\sigma$) and the specimen geometry ($\beta$):

$$K_I = \beta\sigma\sqrt{a} \qquad \text{(Eq.1.1)}$$

The critical stress intensify factor is the value of $K_I$ at which a crack propagates and it is determined by the fracture stress ($\sigma_f$), $a$ and $\beta$ are taken from the specimen. Figure 1.5 illustrates common test specimens for mode I fracture [3].

When shear is involved, mode II fracture also plays an important role in wood structures. Two examples are specimens loaded in flexure and shear bolted connections. In mode II the biggest issue is the lack of a standardized and reliable test to measure fracture toughness [3]. In mode II fracture, the crack propagates parallel to the stress direction, and it should be mentioned there is no practical way to propagate a shear crack cross the grain and it only propagates along the grain (*i.e.*, RL and TL directions) [3]. One difficulty in mode II testing is finding a reliable test method. For monitoring crack propagation, the test needs to additionally

provide stable crack growth. Figure 1.6.a illustrates different specimens that have been used for fracture mode II. The end-notched is more traditional in composites. Another test has been reported that has stable crack growth is four point bending on single end-notched beam which is shown in Fig. 1.6.b [4]. Another problem in mode II testing is measuring crack growth, because the shear mode does not result in easily observable crack opening. This work monitored mode II crack growth using optical detection of crack-tip stress fields.

Besides modes I and II, a crack can be loaded in mixed mode, which is between mode I and mode II. The most common way to test mixed mode is to put an inclined crack in a tension field as illustrated in figure 1.7. For anisotropic materials like wood, however, a crack is more likely to propagate along the minimum crack resistance direction [3]. Wu 1967; studied Balsa wood under mixed mode conditions and proposed the following equation for mixed mode crack growth:

$$\frac{K_I}{K_{IC}} + (\frac{K_{II}}{K_{IIc}})^2 = 1 \qquad \text{(Eq.1.2)}$$

Various researchers have suggested other fracture criteria for mixed mode, which are more general, in which $a$ and b are calibration constants:

$$(\frac{K_I}{K_{Ic}})^a + (\frac{K_{II}}{K_{IIc}})^b = 1 \text{ (Eq. 1.3)}$$

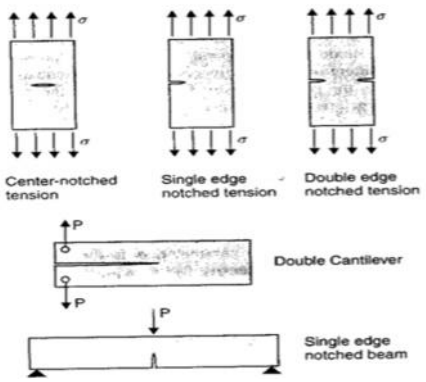


Figure 1.5. Different samples for mode I tests [3]

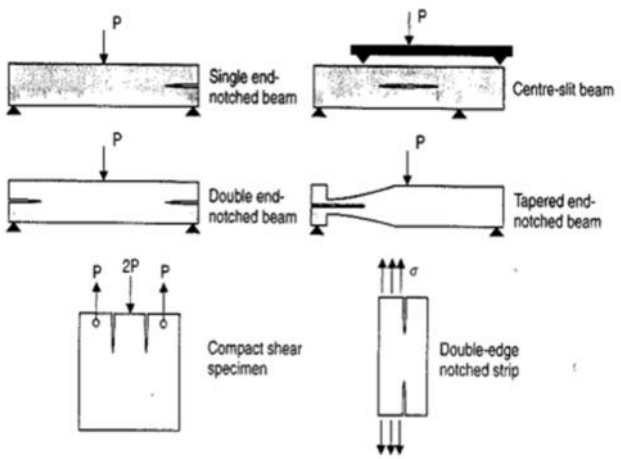


Figure 1.6.a. Different samples for mode II tests [3].

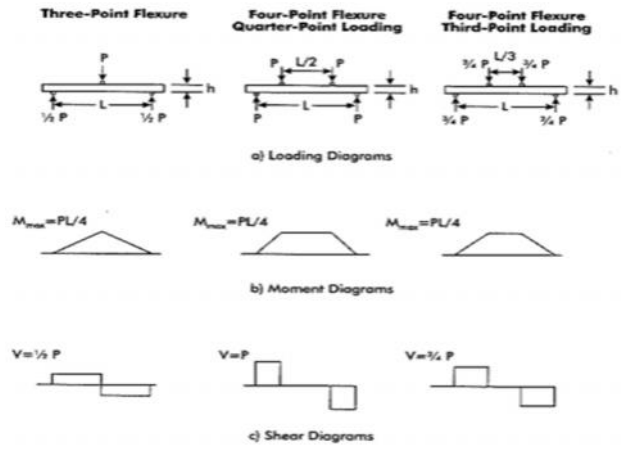


Figure 1.6.b. Four point bending test [4].

*1.5. Previous work on the Fracture of wood:*

Early the work on wood fracture measured the resistance of wood by either static bending or impact bending. Wu 1963, Schniewind & Pozniak 1971, Johnson 1973, and Jeronimidis 1980 applied classical methods of fracture mechanics to wood [5]. Various geometries, like single edge-notch in tension, double notch and center notch in tension, were used and $K_{IC}$ was calculated from load at which crack started to propagate or the sample failed, with use of standard formulae appropriate to each geometry (but possibly not appropriate to wood) [5,6]. Ashby: 1985; used a loading jig in a scanning electron microscope to examine crack propagation and used two

standard test geometries as a function of the crack length and crack orientation. The problem with these tests was they interrupted at 10 intervals to take a micrograph. By this approach fiber bridging is eliminated. Because the assumption is that the unloading load-displacement curve returns to the first point. But, sometimes broken fibers interfere with unloading and complicate the analysis [7]. This effect will be discussed by energy release rate theory.

Ashley 1985; worked on fracture toughness of wood as a function of density and suggested: $K_{IC}=D\ (\frac{\rho}{\rho_s})^2$ where $K_{IC}$ is fracture toughness; ρ is the density of wood, $\rho_s$ is density of cell wall material and D = 20 for crack normal to the grain and D =1.81 for cracking along the grain. This equation suggested the failure strength related to the square of density [5]. The effect of density on fracture energy also was investigated in this project.

*1.6. Crack Propagation in Wood and Wood Composites Including Crack Tip Processes and Fiber Bridging Mechanics:*

Wood and wood composites are materials that develop process zones around crack tips that consist of fiber bridging along the crack. Crack propagation experiments always start with a machined notch and the crack tip of this initial notch has no process zone. When loaded and crack propagation begins, a fiber bridging zone develops. As a result, there are two crack tips, one at the edge of the bridging zone, notch root, $x_{root}$ and one at the actual crack tip at $x_0$ (Fig. 1.7). The length of the developing bridging zone is "$x_0$ - $x_{root}$" [8]. At early stages of crack propagation, the crack tip moves while the notch root remains motionless. In this case, the observed toughness evolves as characterized by a rising R curve (fracture resistance curve). After full development of a bridging zone the two tips propagate together (barring the onset of edge effects) as steady state or self-similar crack propagation with a constant bridging zone length. In this stage, the observed toughness is constant until edge effects influence the process zone [8]. Conventional fracture mechanics can be used to measure fracture toughness, if the developed process zone is small. Larger zones, however, invalidate traditional fracture mechanics methods (*e.g.*, ASTM

E399). Those methods rely on pre-calculated calibration function to find toughness (*e.g.*, stress intensity factor) from failure load [9]. First, all the calibration functions assume stress-free fracture surface. So, they are invalid for cracks with fiber bridging stresses. Second, all fracture methods need information about actual crack length. But, it is hard to visually identify the crack tip when fiber bridging is present. Third, when fiber bridging is significant, the toughness increases as the crack propagates [9].

To solve the above issues, a new energy based analysis has been developed that finds energy release directly from experiments even in the presence of bridging zones. This energy method requires accurate crack growth measurement. The difficulty of observing crack tips when there is fiber bridging can be solved by digital image correlation methods (DIC) that can help to measure strain ahead of the crack. The crack-tip strain field shifts with time, which can be equated to an increment in crack growth needed for determination of R-curve (fracture resistance curve) as a function of crack growth [7-8]. It should be mentioned that fracture energy (G) and stress intensity factor (K) are related by Eq.1.4. in which E is Young's modulus in that direction.

$$G = \frac{K^2}{E} \quad \text{(Eq. 1.4)}$$

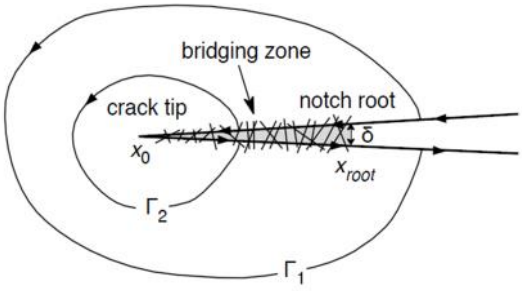


Figure 1.7. Bridging zone around crack tip [8].

*1.7. The energy released calculation:*

As shown in figure 1.8.a, the fracture energy is the area within the triangular area ABC between loading and unloading curves and the fracture toughness is the energy

per unit fracture area. As the crack growth can be calculated from DIC, two equations could be used to calculate fracture toughness:

$$G_c = \frac{P_i(u_j - u_0) - P_j(u_i - u_0)}{2B\Delta a} \quad \text{and} \quad G_c = \frac{P_i P_j (C_j - C_i)}{2B\Delta a}$$

Where $P_i$ is the load when the crack of length $a_i$ starts to propagate at displacement $u_i$ and $P_j$ is the load when crack propagation stops at length $a_j$ and displacement $u_j$. $C_i$ and $C_j$ are the specimen compliances before and after crack propagation; $u_0$ is the displacement at the start of the test and $\Delta a = a_i - a_j$. By this method fracture toughness can be calculated as function of crack length and it include the effect of fiber bridging on fracture energy during crack propagation. Figures 1.9.b and 1.9.c give a schematic view of the method used in this work to find energy release rate [7,10]. Rather than find triangular areas, as in Fig. 1.8 a, Fig. 1.8.b shows the cumulative energy released, which can be calculated as a function of displacement. When this energy is replotted against crack length (which is also measured as a function of displacement), the slope of that curve is the energy release rate as a function of crack length or the R curve [7,10]. This approach is a direct measure of R curve that does not require any assumptions about the specimen or the size of the process zone.

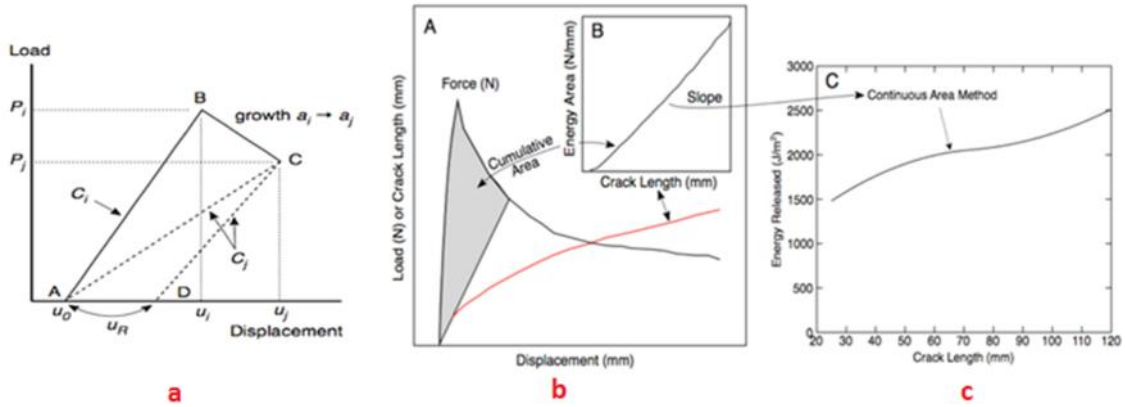


Figure 1.8. (a)The triangular area ABC between loading and unloading curves, (b and c) The schematic picture for energy-released calculation [7].

*1.8. Skin-core interfacial fracture in sandwich composites:*

A sandwich composite is a special class of composite materials that is fabricated by attaching two thin but stiff skins to a lightweight but thick core. The core material is normally low strength material, but its higher thickness provides the sandwich composite with high bending stiffness with overall low density (see Fig 1.9). In sandwich composites, a crack might divert to the interface between core and skin. In this situation fracture energy will be calculated different than fracture energy when crack propagates inside a materials. In order to measure G for a skin-core interface, a three-point bending specimen with a crack between core and skin is often used (see Fig. 1.10) [11]. Skins are usually glued by curing to the core. So, for a full analysis it should be assumed a sandwich composite is compromised of at least five layers; two skins, two glue layers and a core and because of curing (temperature change) it may have residual stresses [11]. The mode mixity of interfacial fracture depends on properties of these layers [12]. The fracture energy for bonding in sandwich composites will be discussed comprehensively in chapter 7.

As it has been mentioned, Balsa wood is used as a lightweight core material in sandwich composites. Increasing use in construction necessitates a better understanding of its mechanical and failure properties. In the present work, mode I and mode II fracture toughness for different types of balsa wood and a sandwich structure (balsa as core and fiber glass as skin layer) were studied experimentally by using load-displacement diagrams and visually acquired crack growth data. Chapter 2 describes materials and methods for raw Balsa tests in mode I and mode II tests. Chapter three has the results for mode I fracture in all directions. Mode II and mixed mode are discussed in Chapter 4. Chapters 5 and 6 discuss the mode I fracture for infused Balsa and Banova (LVL Balsa). Chapter 7 has the resulted the skin/core interfacial fracture toughness of Balsa core sandwich composites.

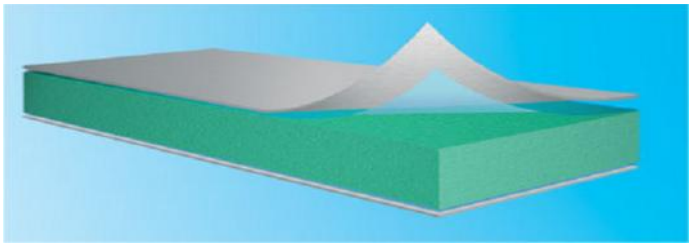

Figure 1.9. Sandwich composites structure.

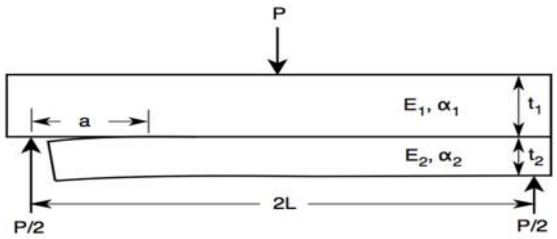


Figure 1.10. Three point bending specimen for testing skin-core interfacial fracture energy [11].

# Chapter 2. Materials and Methods

*2.1. Mode I Tests*

Single end-notch, double cantilever beam specimens were used to measure the fracture energy of balsa wood in the following directions: RL and TL; RT, TR and 45° RL. For the first two directions and 45° RL, the length, width and thickness of specimens were 200, 25 and 25 mm, respectively, with an initial crack length of 75 mm (see Fig. 2.1). In directions perpendicular to the fiber direction (TR & RT) there was no specimen longer than 140 mm because specimens are limited to diameter of trees and extent of specimens cut in diameter direction. Therefore, glued specimen in RT direction was used to propagate crack but all the samples failed from glued part and crack could not propagate. Figure 2.2 shows glued specimen in RT direction. So, measurements for the RT and TR direction were carried out on smaller specimens with length, width and thickness of 135, 40 and 36, respectively; and initial crack length of 35 mm. A total of five specimens were implemented for each direction, two of which were used to study the effects of sharp crack tip created using razor blades. The displacement rate was 2 mm/min using an INSTRON 5443 testing frame.

Crack tips (and crack lengths) were tracked using a DIC camera and the complete load-displacement diagram (LDD) was recorded during stable crack propagation. All data was collected under ambient conditions (about 25 °C and 65% humidity). After tests, sample densities for regions near the crack tip were measured to investigate the effect of density on R curves.

*2.2 Mode II Tests*

The mode II or GII tests were done using a four-point bending method. These specimens were longer than the GI specimens because shorter specimens showed contact deformation at the support-points caused by high loads, which leads to wrong results for GII. In order to decrease load at failure, longer specimens were used to have enough energy release rate at crack tip to propagate crack (see Fig. 1.5.b). The specimens' size were 25 X 25 X 500 mm, crack length was 200 mm and span between loading points above the specimen was 100 mm. The longer span side loading points allowed larger moment with lower force to avoid any deformation at support-points prior to crack growth. In order to further limit deformation at support-points, plateau supports were used to distribute force. Figure 2.3 shows the schematic picture of the specimen. The flexural rate was 3 mm/min using an INSTRON 5443 machine.

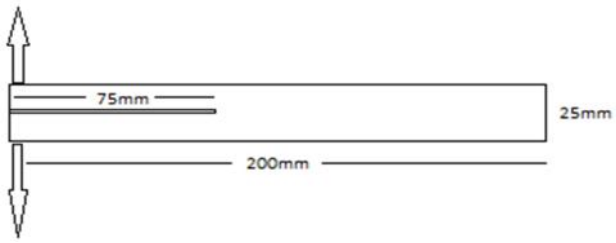


Figure 2.1. Schematic picture for mode I fracture samples.

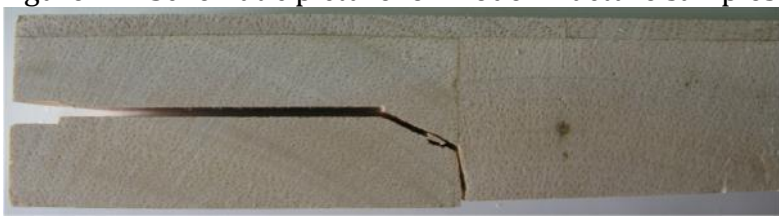

Figure 2.2. Specimen failed in glue line and crack did not propagate in RT direction.

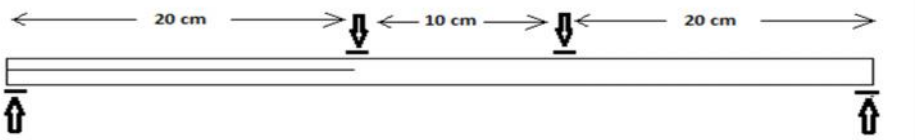


Figure 2.3. Schematic picture of specimen for four-point bending tests.

*2.3 Mixed Mode Cracks*

In some mode I specimens, the crack did not go straight, but instead turned from mode I to mixed mode. In order to find GI and GII percentages finite element analysis (FEA) analysis was used to find mode mixity. The method is described comprehensively in Mode II and mixed mode chapter 4.

# Chapter 3. Mode I Fracture toughness

*3.1. Introduction:*

For fracture in mode I, at it has been mentioned, crack growth is perpendicular to the load direction. In this chapter, Mode I fracture toughness of raw Balsa wood was investigated for both crack growth perpendicular (TR an RT) and parallel (RL, TL and 45˚RL) to the wood fibers direction (45°RL refers to a direction which is oriented 45° from R direction).

*3.2. Mode I fracture toughness parallel to the fiber direction:*

*3.2.1. RL*

Figure 3.1 illustrates the collected R curves for five representative measurements in the RL direction with stable crack growth. Some specimens studied in the RL direction with normal crack tips showed unstable crack growth, leading to unreliable data; they had to be ignored. The curve for sample 1 demonstrates stable crack growth for a specimen without a sharp crack tip, starting at around 50 J/m$^2$ and reaching about 60 J/m2 after a total growth of 15 mm (total crack length was 90 mm). The crack in specimen No. 1 was almost straight (see Fig. 3.2). It can therefore be concluded that the mode I fracture energy, without presence of mode II, was

measured. The R curve stabilizes and flattens after 15 mm into the crack; giving rise to a maximum mode I fracture energy for balsa wood in the RL direction of about 60 J/m2. Because there was little increase in the R curve with crack propagation, there was probably little influence of fiber bridging.

Sample 2, which had a sharp crack tip formed with a razor blade, also had stable crack growth. As seen in Figure 3.1, the onset of the R curve is around 50 $J/m^2$, increasing to about $60J/m^2$ at about 30 mm of crack growth. Up to this point, samples 1 and 2 behaved similarly, after which the curve for sample 2 deviated and increased indicating either fiber bridging or a mode II interaction. Figure 3.3 shows that the crack in this specimen is not straight and deviates from the center line after about 30 mm (105 mm total crack length), which causes mixed mode fracture and/or fiber bridging in mixed mode, and results in an increase in the R curve. This sample will be discussed further in Chapter 4 on mode II and mixed mode failure.

For fracture in specimen RL 3, the R curve starts from 75 $J/m^2$ and increases up to 125 $J/m^2$ after 50 mm of crack growth (total crack length 125 mm). The increase may be because the wood fibers are not completely horizontal in this sample and they act as a barrier against crack propagation due to more fiber bridging. Another possibility, which will be investigated for this sample, is mixed mode. As Figure 3.4 shows, the crack was not straight (horizontal). Also, fracture increases more than the case of pure mode I, which is caused by more fiber bridging, as suggested visually in Fig. 3.4.

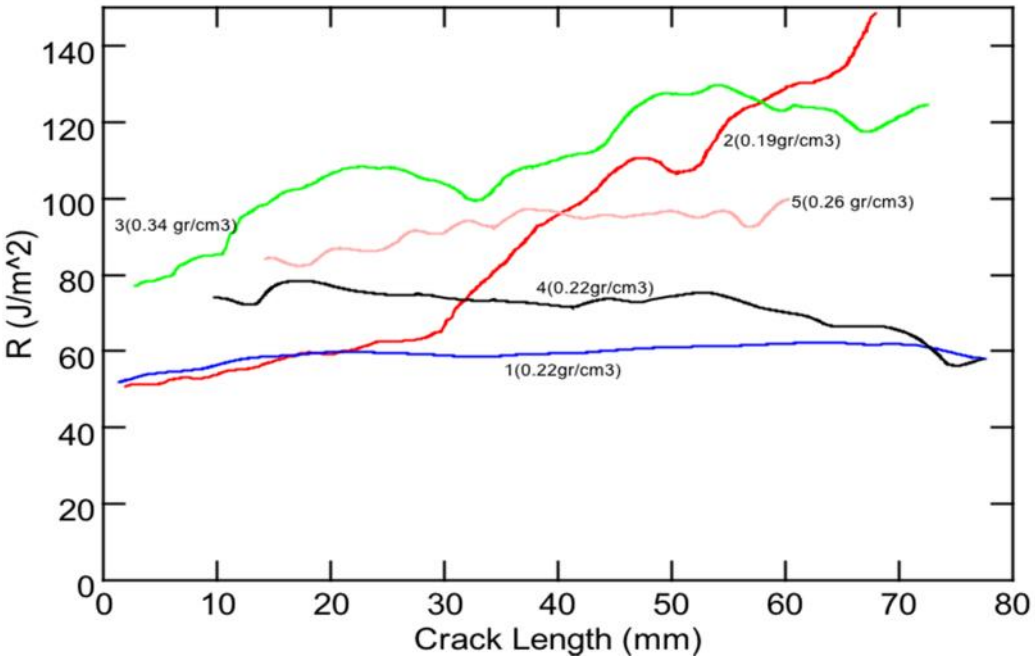


Figure 3.1. R-curve plot for specimens in RL direction.

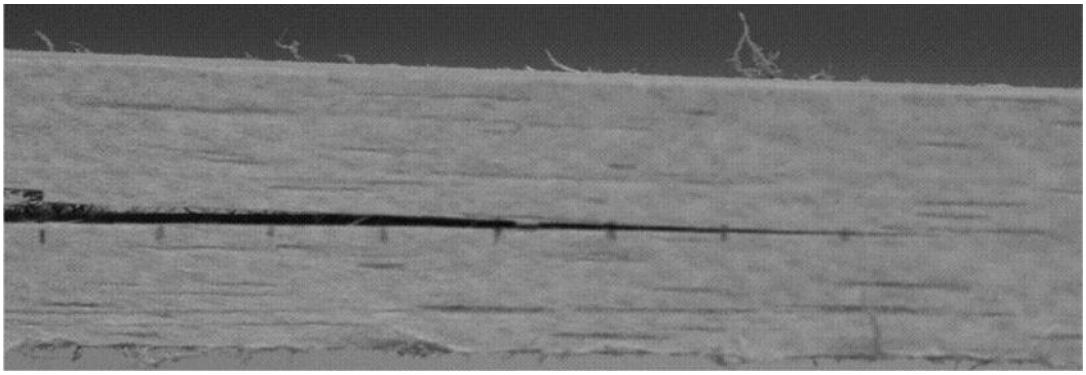

Figure 3.2. Sample No.1 in RL direction.

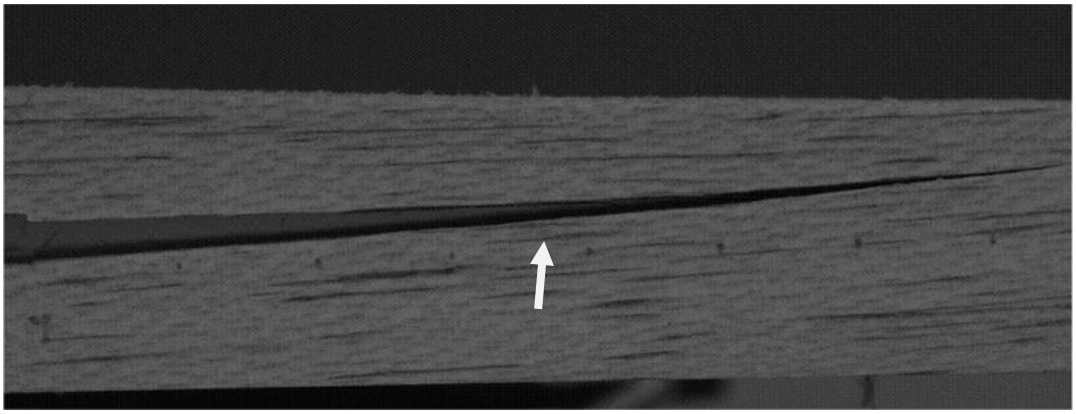

Figure3.3. Sample No.2 in RL direction. Crack turns from horizontal after 34mm growth (total length get 109mm).

Figure 3.4. Sample No.3 in RL direction.

Specimen No. 4 also showed a plateau R curve, which shows almost no fiber bridging in those samples. But specimen No. 5 had higher density and it showed fiber bridging and slightly increasing in R-curve from 80 $J/m^2$ to 100 $J/m^2$.

Density measurement for samples in the RL direction showed that increasing the density in balsa wood, increased the fracture energy increase but may not affect fiber bridging much in this direction and still shows almost flat R curve. So, R curve increasing in samples No. 2 and No. 3 is because of crack deviation and fibers, which are not horizontal and cause fiber bridging. In the other word, samples 2 & 3 are not purely in RL direction because cracks are not going completely parallel to the fiber direction.

If we ignore mixed mode effects here, the samples with lowest density (1, 2, and 4) are mostly flat, except for 2 which may have showed the most crack deviation. The sample with highest crack density had more increase, which may be due to more fiber bridging. It is reasonable that for higher density, which has more fibers, to have more bridging as well.

The Gibson and Ashby scaling argument claims critical K scales as $\rho^2$, which means critical G scales as $\rho^4$. According to this theory, increasing density from .22 to .34 should increase toughness by a factor of (0.34/0.22)^3 = 3.69 or from 60 to 221, which is not observed. These results for a range of densities within a single species show the Gibson and Ashby scaling predictions are not valid for fracture properties.

Furthermore, compared to toughness higher density wood (e.g., Douglas fir [9], Balsa wood has much higher toughness then predicted by Gibson and Ashby scaling.

*3.2.2. TL*

Three R curves for TL fracture are shown in Fig. 3.5. In the TL direction, sharp-tip samples did not show significant difference to samples with normal cracks; all samples will be discussed together. In sample 1, crack is almost straight during propagation. The R curve starts from 140 J/m$^2$ and goes up to 150 J/m$^2$ (Fig. 3.5) after crack growth of 80mm (Total length 155mm). The low slopes show that in The TL direction, balsa does not have considerable fiber bridging effects. The overall toughness for TL, however, was more than twice the RL toughness at comparable density. The density for this specimen was 0.227 gr/cm$^3$

For sample 2, density was 0.264 gr/cm3. The R curve starts from 140 J/m$^2$ and goes up to 150 J/m$^2$. After crack growth of about 35 mm, (a total crack length of 110 mm), fracture energy gets almost constant. The specimens broke after the crack growth of 55 mm. The results were nearly identical to sample 1.

For sample 3 the R curve starts from 140 J/m$^2$, almost similar to other samples, and the curve goes up to 155 J/m$^2$, the slope of the R curve is almost the same as that of No. 2, by crack growth. After about 50 mm of crack growth (125 mm total crack length) the slope changed. Crack path for this sample showed that the crack deviates after 50 mm of crack growth, which may indicate a contribution of mixed mode fracture to the R curve. Alternatively, it may be showing more fiber bridging than samples 1 & 2. The difference between these samples is discussed in “mode II and mixed mode“ chapter 4.

Density measurement for samples in TL direction showed that density had little effect on initial fracture toughness. It is possible that density played a role in fiber bridging. The sample with largest increase in R curve was the sample with the highest density. This observation is similar to the RL fracture observations. The consistency in results for different densities again shows that Gibson and Ashby scaling is too simplistic to predict fracture variations between wood specimens.

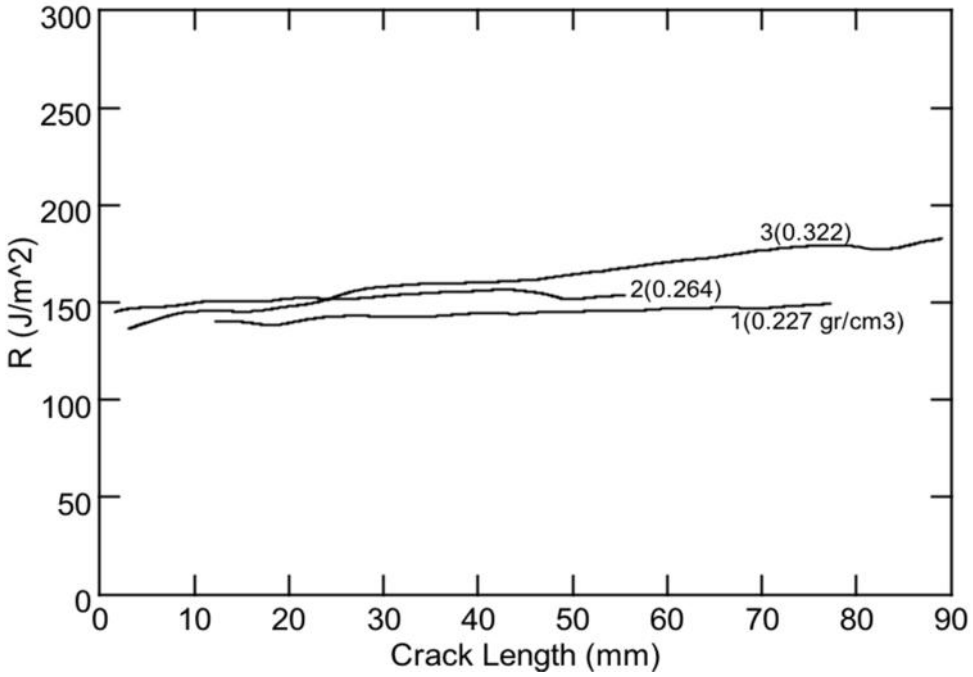


Figure 3.5. R-curve plot for specimens in TL directions.

*3.2.3. 45°RL*

The 45°RL direction specimens had variable results. Two specimens (No. 1 and 2) were used without razor blade notching or without a sharp crack tip. In sample No. 1, when the crack started to grow, it jumped to 20mm (fast growth) and after getting to about 30 mm crack growth, the R-curve was around 100 J/m$^2$ with almost no fiber bridging. The crack then started to grow faster and, as it is obvious in Fig. 3.6, the R-curve drops and that is because in that area, the sample had lower fracture energy. Figure 3.6 shows R-curves for sample No. 2 that started from 105 J/m$^2$ and showed no signs fiber bridging (i.e., they are flat). After around 40 mm crack growth it dropped because of what was mentioned before. These two samples had different densities, which suggests the density may not have much effect on the R curve in the 45°RL direction.

Two other samples were chosen from another tree's block and a razor blade was used to create sharp crack tips. Figure 3.6 shows R-curve plots for these two samples (sample 3 density was 0.275 g/cm$^3$ and sample 4 density was 0.296 g/cm$^3$).

For sample 3, fracture energy starts from 160 J/m$^2$ and goes up to around 205 J/m$^2$ by about 40 mm of crack growth (115mm total length) and after that the R curve was flat. This shows more fiber bridging compared to the other block (in samples 1 and 2). Figure 3.7 shows crack propagation for sample 3 is mostly horizontal or stays in pure mode I. For sample 4, the R-curve starts from almost 160 J/m$^2$, which is similar to sample 3 in this direction, and goes up smoothly, but after the crack reaches about 22 mm of crack growth (total crack length 97 mm) crack turns from horizontal direction (see Fig. 3.8). At this same point, the fracture energy goes higher than the R-curve plot for sample 3. Furthermore, some 45RL direction specimens had higher fracture energy than both RL and TL direction, which was unexpected. These two samples also will be discussed further in the mode II and mixed mode chapter 4 to find mixed mode interactions.

Razor blade sharpening in fracture testing is used to eliminate blunt starting point for load-displacement curve, which may cause higher initial fracture energy and promote unstable crack grows immediately after initiation. The results show in the 45°RL direction sharp crack tip does not affect starting points of R-curve. In fact, the specimens that had sharp crack tips needed *higher* energy to start crack initiation, which is contrary to the typical comparison of sharp to blunt cracks. In these experiments, tree-to-tree variations (samples 3 and 4 compared to samples 1 and 2) were probably much large than crack sharpness effects. The local structural diversity of wood is probably sufficiently able to initiate cracks without needing razor blade sharpening that is more crucial in less heterogeneous materials.

Another possible reason samples 3 and 4 had higher fracture energy, is that the fibers in those samples were not completely horizontal. Because of this orientation, the crack had to cut cellulose to propagate. Therefore, the fibers acted as a barrier against crack propagation, increased fracture toughness, and increased fiber bridging.

Density measurement for the 45°RL direction specimens showed that increasing density tended to increase fracture energy. The increase is still less than predicted

by Gibson and Ashby scaling. Therefore, samples with higher density showed higher fracture energy and more fiber bridging, But cellulose direction, as mentioned before, also affected fiber bridging in this direction.

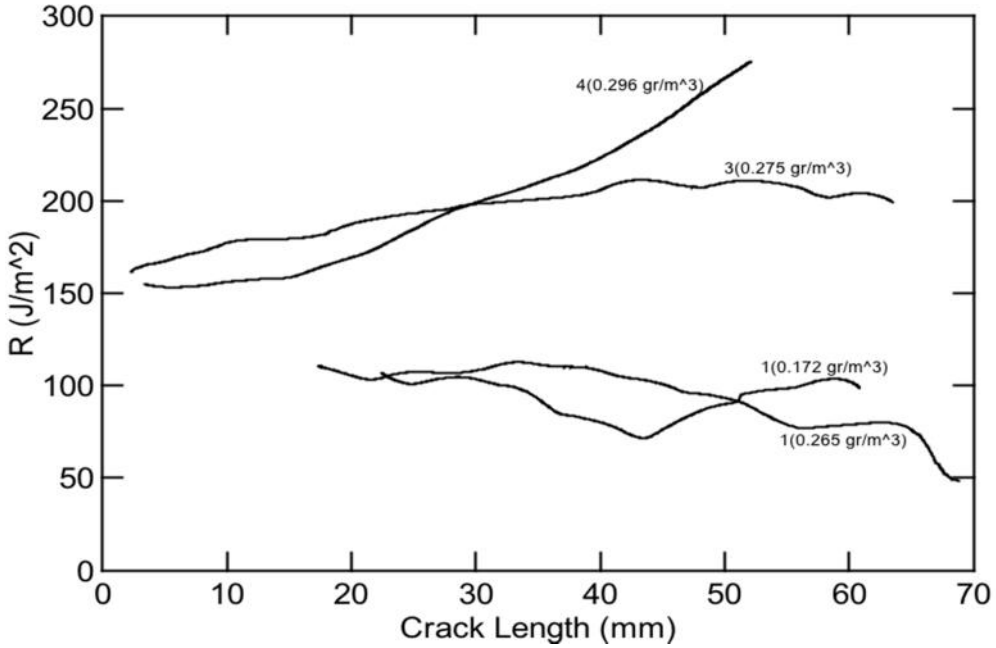


Figure 3.6. 45°RL samples R-curve. Specimens with 0.172 and 0.264 gr/cm$^3$ had crack without using razor blade, for two other razor blade has been used to make sharp crack tip.

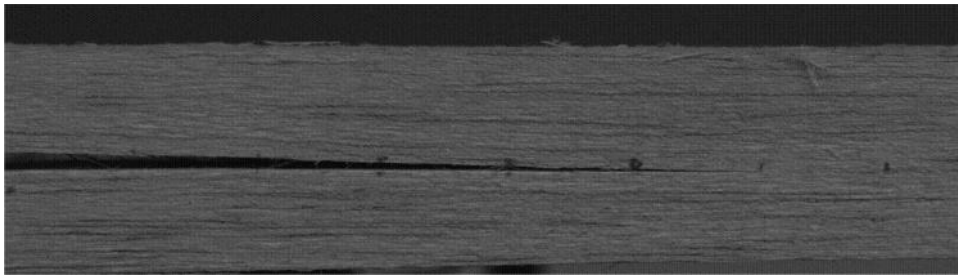

Figure 3.7. Sample No.1 in45°RL without sharp crack tip.

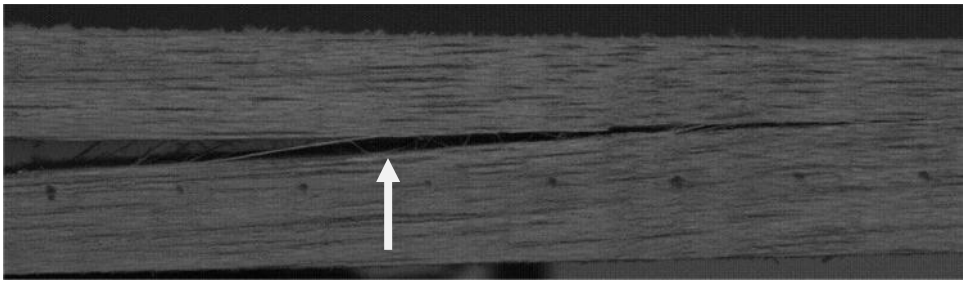

Figure 3.8. Sample No.4 in45°RL with sharp crack tip; Crack turns from horizontal axis (mode I) after reaching around 25mm crack length.

*3.3. Mode I fracture toughness Perpendicular to Fibers (TR & RT):*

In the TR direction, it was impossible to induce crack growth. In the other word, by loading in the TR direction, the crack always turned. So, that the specimens broke in the RT direction.

In the RT direction, stable crack propagation took place. Wider specimens had been chosen (36-40 mm), as it was difficult to induce straight propagation in the RT direction due to rapid turning and sample failure. R curves in this direction start from different points. Figure 3.9 shows R-curve for samples in RT direction. No. 1 started from 85 $J/m^2$ and went up to 150 $J/m^2$ with a crack length of 35 mm. The crack in the second sample started from 100 $J/m^2$ and went up to 200 $J/m^2$ reaching a total crack length of 60 mm. Samples 3 and 4 showed almost the same starting points, 180 $J/m^2$, but turns in No. 3 after approximately 10 mm of growth, resulting in a different slope. The crack in sample No. 5 started from 380 $J/m^2$, which is 3-4 times higher than the other samples. As Figure 3.9 shows, the R curve slopes are almost higher than R-curves parallel to the fibers direction (TL, RL and 45°RL). Therefore, it can be concluded that in the RT direction fiber bridging has the same effect on fracture energy and is considerably higher than in the RL and TL directions.

As figure 3.9 illustrates, density in RT direction has considerable effect on crack initiation and fiber bridging. Even small increase in density causes higher fracture toughness. Just sample No. 3 is not following this rule and that happened because, as figure 3.10 shows, the crack in this sample deviated from horizontal axis and R-curve is for mixed mode. Also as R-curve for sample No. 5, which had highest density in RT direction, shows fiber bridging in RT considerably higher than other samples in this direction. So, data shows in RT direction for balsa wood that density plays an important role on fracture toughness and fiber bridging.

As it has been mentioned, for sample No. 3 its R-curve was higher than No. 1 and No. 2 (we expected to be lower because it had lower density). The reason for that is, as figure 3.10 shows, the pre-crack is not completely in the RT direction for mode I and

it is mix of RT and TR direction. Because crack cannot propagates in TR direction it acts as a barrier against propagation, which causes to increase in the starting point of the R_curve for mode I. Furthermore, as crack just goes in RT, it turn to mixed mode propagation in order to avoid the TR direction.

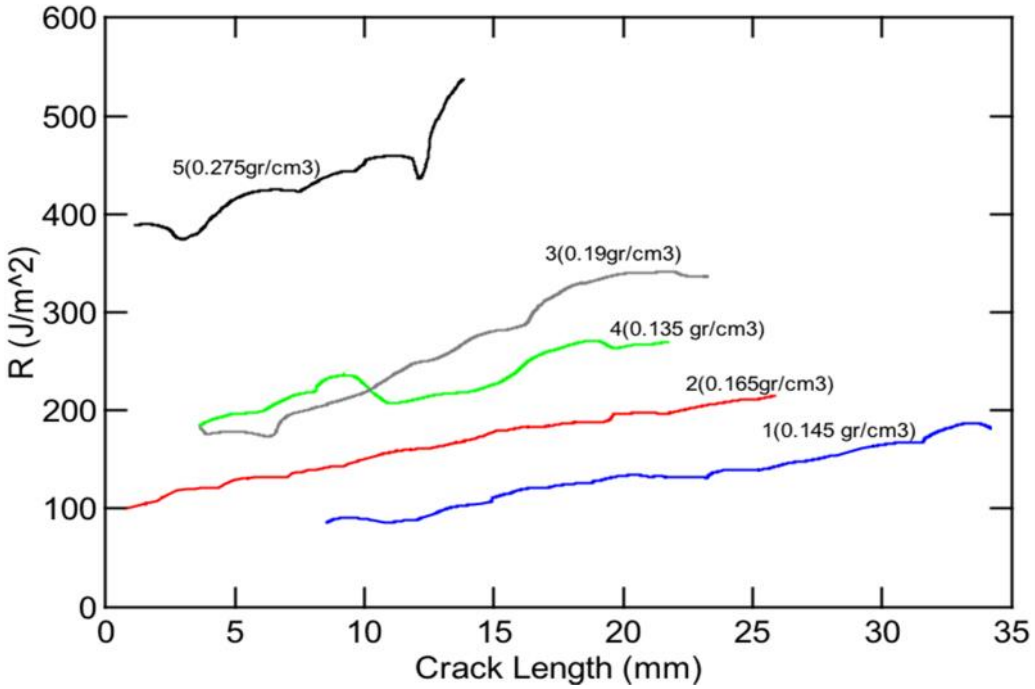


Figure 3.9. R-curve plot for specimens in RT directions.

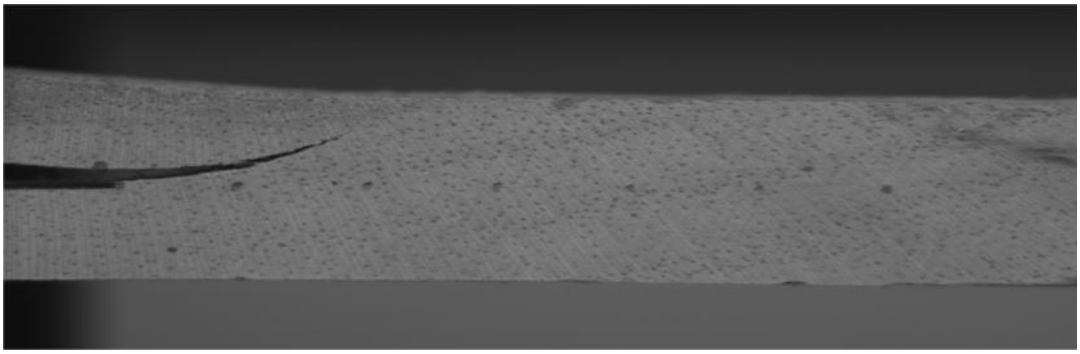

Figure 3.10. Sample No.3 in RT direction.

# Chapter 4. Mode II and mixed mode Fracture toughness

*4.1. Introduction:*

This chapter discuses experiments needed for finding fracture toughness in mode II or GII and considers mixed mode fracture for mode I crack that deviated from the

specimen mid-plane. As has been explained, in mode II fracture, the crack propagates parallel to the loading direction. Four-point bending showed more stable crack growth among different test tried for Mode II. In order to find crack length in this test, specimens were prepared for crack growth in both RL and TL directions and speckle patterns along with VIC software to find the crack tip. This optical method was used because in mode II, there is no crack opening and crack tip was invisible. The DIC method made it possible to observe shear strain ahead of the crack tip. The assumption was that crack tip was located at a constant distance from the location where there is 1-2% shear strain (depends on samples). So, the difference between the points was Δa or the change in crack length. Figure 4.1 shows shear strain and how the difference between points with 1% shearing, were collected to find Δa. The results for Δa are relatively insensitive to the specific shear strain chosen (e.g., the 1% strain).

After finding the results for mode II, the samples, which had crack deviation in mode I in chapter 3, were further investigated for mode mixity by using FEA of an off-center crack.

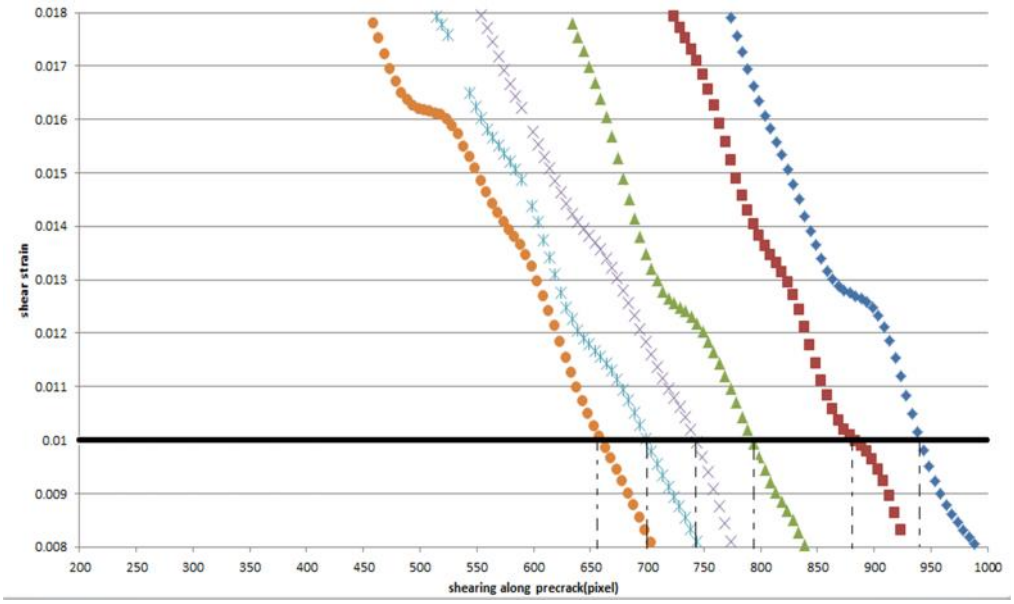


Figure 4.1. The difference between points with 1% shearing, were collected to find Δa.

### 4.2. Mode II Fracture

For RL specimens, as shown in Fig. 4.2, the mode II R curve starts from 360 J/m$^2$ and reaches 400 J/m$^2$ while crack grows less than 10 mm. After that, the curve shows a plateau curve, as we expected for Mode II. The assumption for mode II is that there is no fiber bridging around the crack tip. Because there is no opening at the crack tip and shear stress causes crack propagation. With no fiber bridging effects, we expect a flat curve for GII. At the start, the R curve was not at the plateau, but it grew sharply and then reached a flat shape. One reason for that may be the pre-crack. As Figure 4.3 shows, the space created by saw cut caused the top and bottom half of the specimen to initially not be in contact, which may affect loading state. Therefore, when crack first starts to propagate it may not be pure mode II. After some crack growth the space closes, the toughness increases and turns to pure mode II. Another possibility is that the crack starts in the middle of one of the external loading points, possible creating mixed mode stress state. Once it clears the loading point the loading is more pure mode II.

In the TL direction, the R curve plot for mode II showed almost the same behavior as mode II in the RL direction. The R curve started from 350 J/m$^2$ and grew until about 390 J/m$^2$, then showed a flat curve around 390 J/m$^2$.

Figure 4.2 also shows mode I TL and RL fracture for comparison. The mode II toughness is much higher that the mode II toughness, although the difference between RL and TL in mode II are much smaller. Because of the difficulty in measuring crack length in mode II, these are the first mode II R curves we know of for solid wood of any species.

### 4.3. Mixed Mode Fracture

During mode I crack propagation, in some samples, the crack deviated from mid plane and fracture energy was not purely mode I. In this section mode mixity was investigated to find how GI and GII interact during crack propagation and to consider the role of fiber bridging when interpreting such experiments.

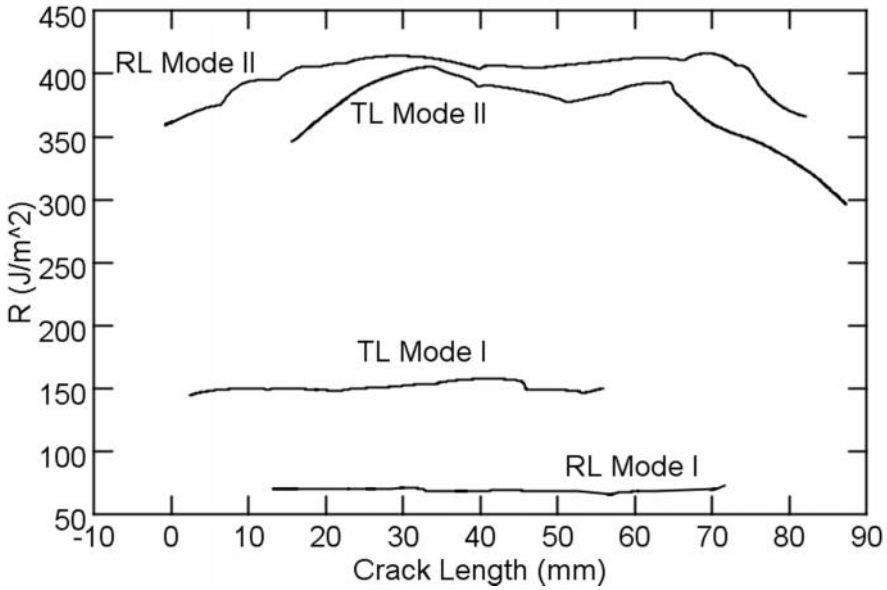


Figure 4.2. R-curves for mode I and Mode II RL and TL directions.

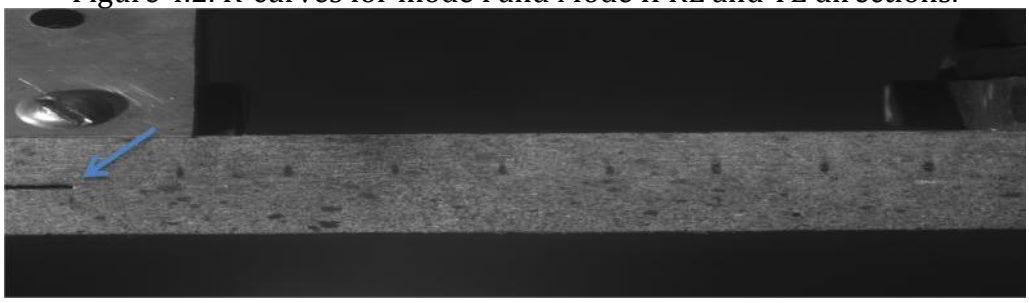

Figure 4.3. Pre crack's width caused space between above and below of mid plane.

In the TL direction, the mode I R curve for Balsa wood showed almost no fiber bridging when crack was completely perpendicular to the applied force direction. The crack deviated in TL sample No.3. For analysis, the sample thickness h at a given crack length was divided into $h = h_1+h_2$ where $h_1$ is distance from crack to farthest surface and $h_2$ is distance to closer surface. Next, FEA results by crack closure were used to tabulate mode mixity, $\varphi = GI/G$, as a function of the ratio $h_2/(h_1+h_2)$, which varies from 0 (crack at surface) to 0.5 (crack in the middle). Table 4.1 shows different $\varphi$ for different $h_2/(h_1+h_2)$ ratio by FEA analysis. The total G is the value we measured by energy experiments. The amount of that G that is mode I is $\varphi$ *G where $\varphi$ depends on $h_2/(h_1+h_2)$ and found by FEA analysis. So, steps to find GII vs. GI during propagation were:

1. Find G from fracture analysis results for any given crack length
2. Look at picture and find $h_1$ and $h_2$ at that crack length and calculate $h_2/(h_1+h_2)$
3. Find φ for that ratio by interpolation FEA results at selected $h_2/(h_1+h_2)$ ratios
4. Find GI = φ * G
5. Find GII = G - GI = (1-φ) * G
6. Plot GII vs. GI for several points along the curve.

Table 4.1. Different φ for different $h_2/(h_1+h_2)$.

| $h_2/h$ | 0.2 | 0.22 | 0.26 | 0.3 | 0.32 | 0.36 | 0.4 | 0.42 | 0.48 |
|---|---|---|---|---|---|---|---|---|---|
| φ | 0.706786 | 0.72407 | 0.76489 | 0.812206 | 0.837434 | 0.889083 | 0.937531 | 0.958403 | 0.9972 |

Figure 4.4 shows GI vs. GII in TL sample No. 3. GI in TL direction decreases gradually from 155 J/m2 to 146 J/m2 while GII increases up to 37 J/m^2. So, total R curve increases in this sample. In theory, when there is no fiber bridging, by increasing crack deviation from mid plane GI will decrease and GII goes up. In this sample, No. 3 in TL direction, FEA analysis showed still 80% of fracture is in mode I (in maximum deviation). Also as results for mode II in TL direction showed, GII was 390 $J/m^2$. So, by data from this sample, it is hard to get full equation for GI vs. GII. The additional of more points to the mixed-mode curve would require new tests using different specimen geometries with greater mode II component.

In the RL direction, samples No. 2 and No. 3 had crack deviation during propagation. Figure 4.5 shows GI vs. GII plots for these two samples. GI R-curves for these two samples showed they have fiber bridging, before the crack starts to deviate, during pure mode I fracture. So, it is expected to still have fiber bridging when crack still propagates, even though it deviates from mid plane. As figure 4.5 shows, GI still increases even after turning from mode I to mixed mode. Therefore, GII vs. GI plot for these to samples are not what was expected, from theory, and by increasing GII, in mixed mode fracture, GI increases as well. A possible explanation is that GI is

increasing due to fiber bridging and the mode I component shows that increase, but part of the increase in $G_{total}$ is due to GII as well.

Figure 4.6 shows GI vs. GII plots for sample No. 4 in in 45°RL direction. By increasing crack deviation GII increases as has been expected. But, GI also increases, perhaps because of fiber bridging. As you can see, in Fig. 3.8, fiber bridging exists. Unlike conventional GI vs. GII curves, fiber bridging can cause both GI and GII to increases during crack propagation.

For sample No. 3 in the 45°RL direction, GI starts to decrease, by increasing crack deviation, after reaching a maximum (204 $J/m^2$). The reason is that, when the R-curve (in mode I) reaches plateau shape, fiber bridging does not cause further increase in fracture toughness of sample. Then after reaching the maximum fracture toughness in mode I, by increasing crack deviation, GI decreases while GII increases. Therefore, for this sample, GI vs. GII plot agrees with conventional plots because crack only started to deviate after reaching maximum toughness in mode I.

The last sample for checking GI vs. GII was sample No. 3 in the RT direction. As figure 4.7 shows GI still is increasing, though GII increases, by crack deviation and as has been mentioned above, that is because of fiber bridging during crack propagation.

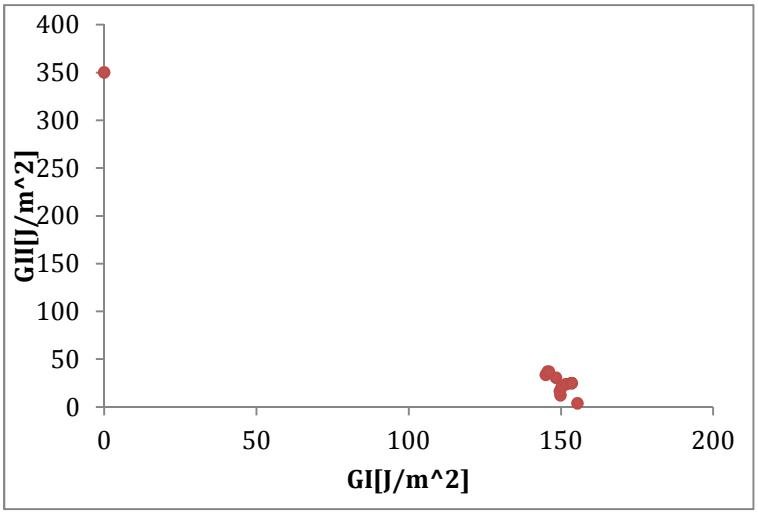


Figure 4.4. GII vs. GI for sample No.3 in TL direction.

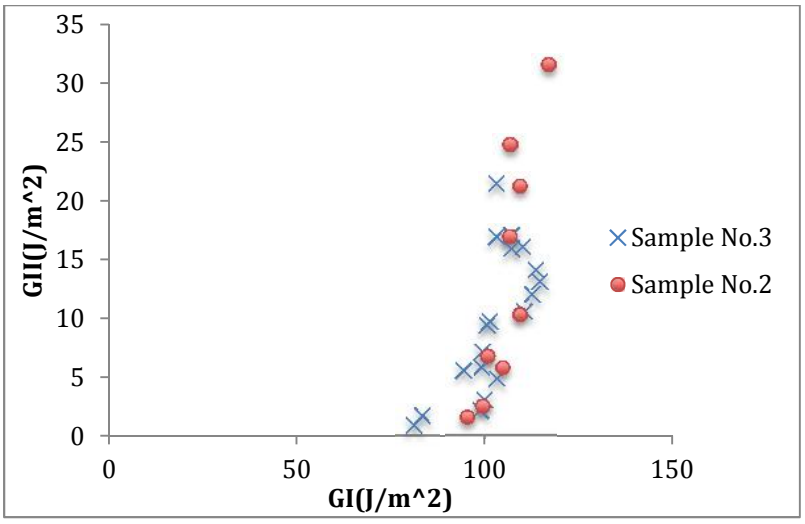


Figure 4.5. GII vs. GI for RL samples.

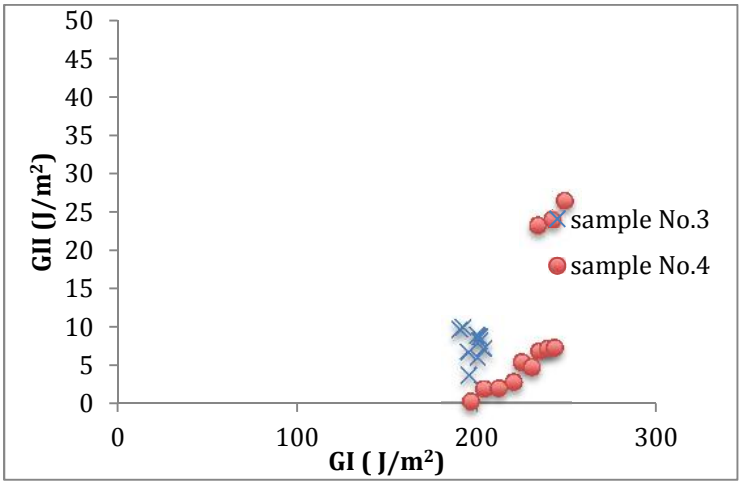


Figure 4.6. GI vs. GII plots in 45°RL direction.

A hypothesis consistent with all these results is that fiber bridging primarily causes an increase in GI. The pure mode GII curves show little or no fiber bridging effects. When a mode I crack propagation experiment deviates from the mid-plane, the fracture becomes mixed mode. If there was no fiber bridging, the expectation in most materials is that the GI part would decrease as the GII part increases. But here, the sequences of points are from crack propagation experiments. In each test the GI part may increase due to fiber bridging. If the crack deviation occurs while the fiber-bridging zone is still developing, it is possible for GI to increase even as GII increases (see Figs 4.5 and 4.6). By subtracting off the GII part, the curves may show a more

accurate picture of fiber bridging. If the fiber bridging zone is absent or already fully developed, then the curves instead show GI decreasing as GII increases (e.g. see Figs 4.4 and 4.7). A general equation for relation between GI and GII from section 1.4 is:

$$\left(\frac{K_I}{K_{Ic}}\right)^a + \left(\frac{K_{II}}{K_{IIc}}\right)^b = 1 \quad \text{Or} \quad \left(\frac{G_I}{G_{Ic}}\right)^m + \left(\frac{G_{II}}{G_{IIc}}\right)^n = 1$$

In this prediction for GI vs. GII curve the assumption is that there is no change in amount of $G_{IC}$ or $G_{IIC}$ during crack deviation. But fiber bridging during crack propagation causes an increase $G_{IC}$ and this increase, shifts GI vs. GII curve to the higher amount in GI axis. Then if sample also showed crack deviation during propagation both GI and GII will increase. Figure 4.8 shows shifts in GI vs. GII plot at fixed levels of fiber bridging. After full development of a bridging zone (see chapter 1.6), the experiments should follow the last curve with max $G_{IC}$. The symbols show the schematic GI vs. GII curve for this kind of material. As the crack propagates the experiments shift to different Gi vs GII curves. So, it is possible to interpolate experimental results (e.g. see Figs 4.5 and 4.6) by this hypothesis.

Overall, crack deviation only introduces a small component of GII and thus is not a good method to map out the full mixed mode fracture properties of Balsa wood. The results are consistent with mode II results (see Fig. 4.4), but more experiments are needed to fully explore the GI vs. GII curve. The results here also show that the curve may shift depending on the amount of fiber bridging when the values are recorded.

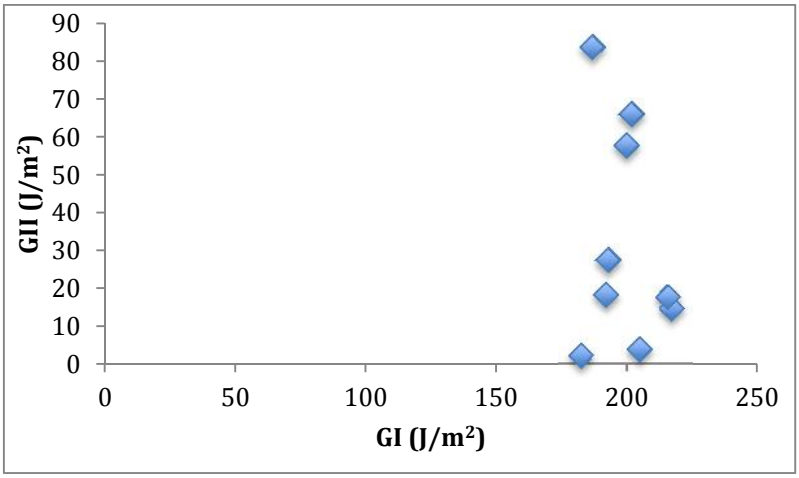


Figure 4.7. GI vs. GII plot for sample No.3 in RT direction.

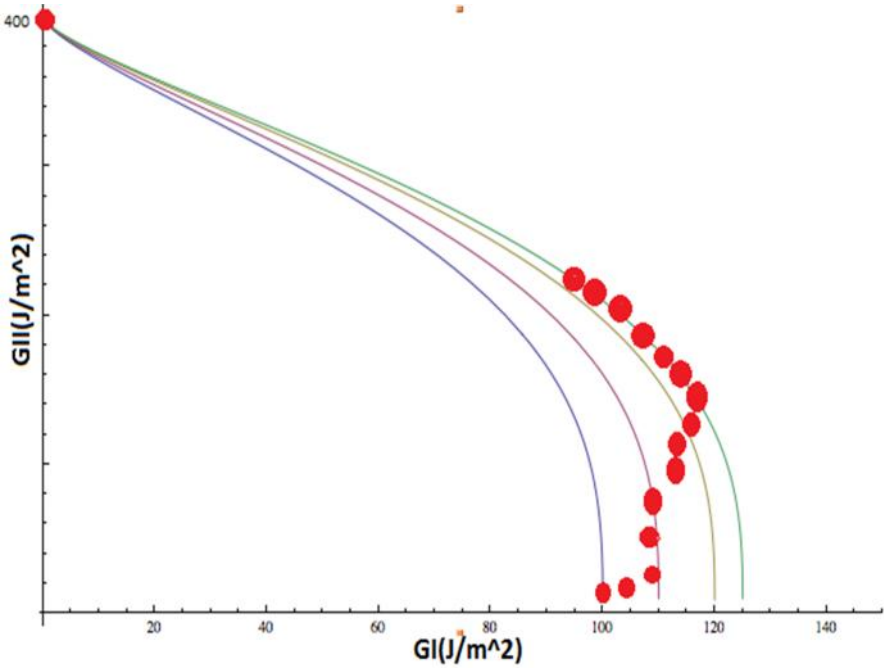


Figure 4.8. Schematic GI vs. GII curve for samples with fiber bridging during crack propagation.

# Chapter 5. Infused Balsa

## *5.1. Introduction*

Balsa wood has porosity in its structure (see chapter 1.2). These porosities cause moisture absorption, which can affect properties of Balsa in different application. For instance it can change mechanical properties of a Balsa core in sandwich panels. Also, more resin will be wasted during bonding with the skin in sandwich panels. In order to decrease moisturizing and have better bonding with skin (while using less resin for bonding), it is possible to impregnate Balsa wood with resin before bonding. In other word, using impregnated Balsa in core of sandwich panels rather than raw Balsa wood and it should be mentioned the density of infused Balsa is not have much different from raw Balsa (1-20% increase in density). Even if Balsa is not infused, it may become infused by the bonding process by the resin used to bond the skins to the core. In this chapter, the fracture energy of infused (or impregnated) Balsa wood and effect of the amount of resin impregnation have been investigated.

*5.2. Materials and methods*

Balsa blocks with different densities, varying from 0.2 gr/cm$^3$ to 0.35, were impregnated by liquid vinyl ester resin under vacuum. This resin was dyed blue to see the resin distribution. The density of each sample was measured around the fracture surface in order to find the effect of resin on fracture toughness. In this chapter blocks with low, medium and high density were chosen in order to measure mode I fracture toughness. The size of the blocks was 55X55X250 mm and were the same as blocks for raw Balsa in mode I direction (see chapter 2). It was assumed that the density is constant in each block. 3A Composites Company performed the resin infusions and provided all samples.

*5.3. Mode I fracture energy in infused RL:*

Four different impregnated samples will be discussed for RL direction crack propagation. Figure 5.1 shows R-curves for the four different samples in this direction. For sample No.1 the density before impregnation was 0.35 gr/cm$^3$ and after impregnation the density around the fracture surface was 0.41 gr/cm$^3$. As its R-curve shows, the fracture energy starts from 100 J/m$^2$ and it is constant until the crack reached 30 mm; after that it increased to 125 J/m$^2$ when crack propagated to 60 mm and then decreased to 100 J/m$^2$. The fracture energy of infused balsa in RL direction is higher than regular balsa with the same density, *e.g*., sample No.1 in RL direction (figure 3.1), and R-curve shows no fiber bridging in first 30 mm crack growth. As figure 6.2 shows, the crack did not deviate from center and it was straight. There are two passible reasons for this increase in R-curve. First, fiber bridging starts after 30 mm crack growth. The fracture surface is smooth and there are few rough places, which could be an evidence for fiber bridging. Figure 6.3 shows fracture surface of sample No. 1 infused RL. The other possibility is that the fracture surface area is bigger than what has been calculated (the assumption was that surface area was the crack length times the specimen width, which may change is surface roughness changes). So, an increase in roughness could cause the R-curve to rise in this area.

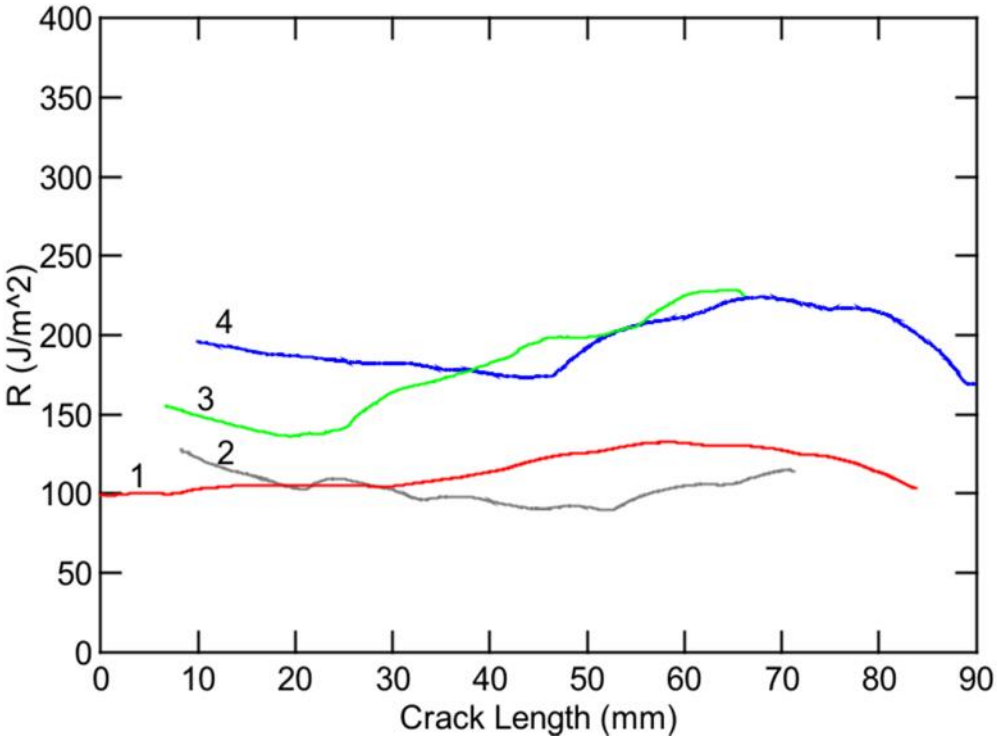


Figure 5.1. R-curve for infused balsa samples in RL direction.

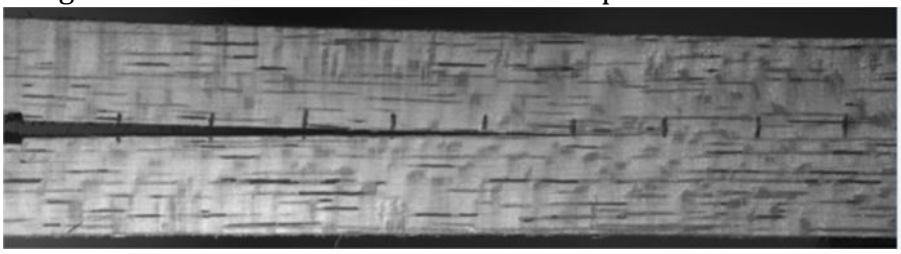

Figure 5.2. Crack path in sample No1 infused RL.

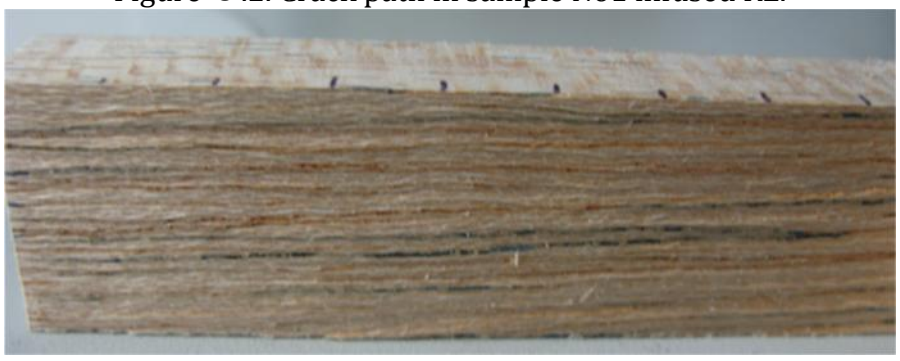

Figure 5.3. Fracture surface for infused RL No.1 sample.

The density for sample No. 2 before and after impregnation was 0.21 gr/cm$^3$ and 0.25 gr/cm$^3$, respectively As the R-curve for sample No. 2 shows (see Fig. 5.1), fracture energy starts from 125 J/m$^2$ and comes down to 100 J/m$^2$ and shows

plateau behavior in R-curve; it starts to rise again after 50 mm crack growth. As figure 6.4 shows this sample also had a smooth facture surface with almost no fiber bridging and the reason for higher fracture energy could be the resin concentration around fracture surface in that area. Also, R-curve goes up after 50 mm crack grows because the crack deviates from the center and after that R-curve shows mixed mode fracture energy. Figure 6.5 shows the crack path for sample No. 2 in this direction.

For sample No. 3 the density was 0.28 gr/cm$^3$ and 0.35 gr/cm$^3$ before and after impregnation, respectively. The R-curve for this sample (see Fig. 5.1) starts from 150 J/m$^2$ and goes up to 230 J/m$^2$ after crack propagation. The crack did not deviate during propagation as figure 6.6 shows and the fracture energy is almost pure mode I. Also figure 6.7 shows the fracture surface for this sample is rougher than samples No. 1 and No. 2, which shows more fiber bridging in this sample and may account for the larger increase.

Figure 5.4. Fracture surface for infused RL No.2 sample.

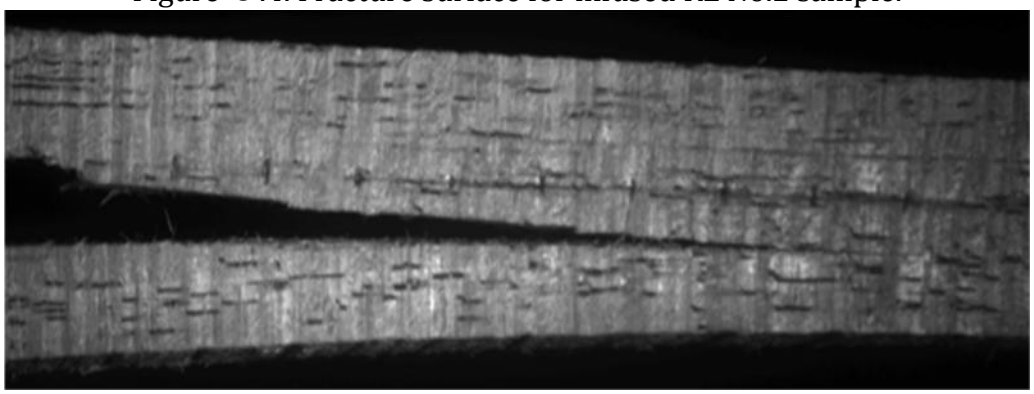

Figure 5.5. Crack path for sample No.2 infused RL.

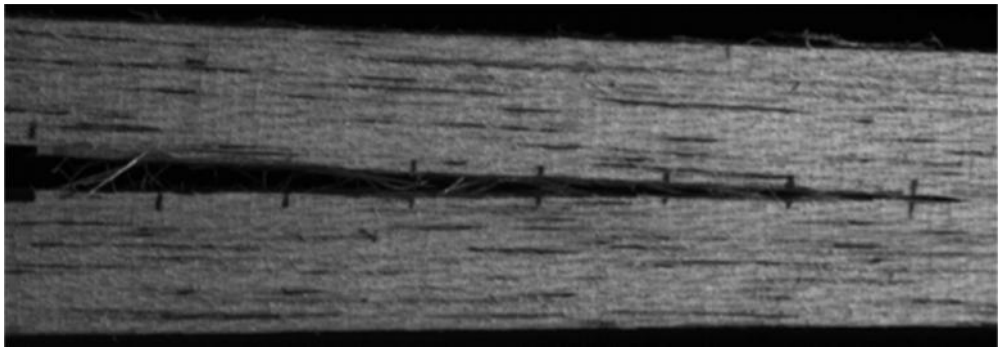

Figure 5.6 Crack in sample No.3 infused RL.

Figure 5.7. Fracture surface for infused RL.3 sample.

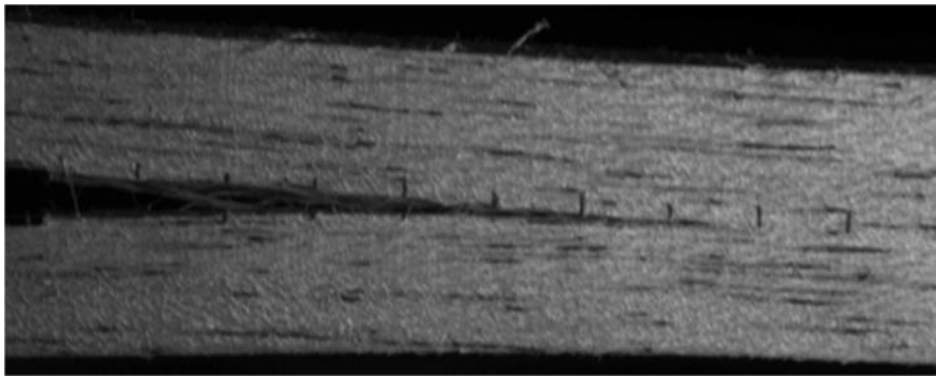

Figure 5.8. Crack path in sample infused RL No.4.

Figure 5.9. Fracture surface for infused RL No.4 sample.

In sample No. 4 the density before and after impregnation was 0.28 gr/m$^3$ and 0.27 gr/cm$^3$, respectively. These numbers show the density was not constant in this block and sample might have pores inside of that which was eliminated before infusion. The R-curve for this sample was higher than other samples in this direction and started around 200 J/m$^2$ and came down to 170 J/m$^2$ and finally goes up to 230 J/m$^2$ by crack propagation. Figure 6.8 shows crack propagation in this sample and fiber bridging is obvious. Also, as figure 6.9 shows fracture surface is rougher which is another reason for fiber bridging in this sample. The reason for the starting point in the R-curve being higher than sample 3 could be more resin concentration around the crack starting point in sample No.4. Another reason for higher starting point in R-curve for sample No. 4 is that the fracture surface was jagged (it was not flat), As figure 6.9 shows, which was not calculated during R-curve calculation. So, the fracture energy is lower than what was calculated in this sample, though R-curve in this sample still is higher than others. It should be mentioned that blue colored lines on fracture surfaces shows resin infusion. As figure 6.9 shows sample No. 4 has more surface resin than No. 1 and No. 2 samples and it causes higher fracture energy.

All results for Infused Balsa in the RL direction showed that the resin infusion causes an increase in fracture energy and fiber bridging. Furthermore, samples with more impregnated visible on the fracture surface had higher fracture energy.

*5.4. Mode I fracture energy in infused TL:*

Four samples for TL fracture will be discussed. Figure 6.10 shows the R-curves for impregnated samples in TL direction. For Sample No. 1, the density before and after impregnation was 0.23 and 0.26 gr/cm$^3$, respectively. In this sample, the R-curve starts from 120 J/m$^2$ and goes up to 300 J/m$^2$. The fracture surface is shown in Fig. 6.11. As it shows the fracture surface is not plateau after crack reaches 15 mm. So, surface is bigger than what has been assumed for R-curve calculation. So, R-curve rose because of miscalculation in fracture surface area. Also fracture surface is rough which is evidence for fiber bridging. Regular Balsa did not show considerable fiber bridging in TL direction but impregnated TL showed fiber bridging during crack propagation. Figure 6.12 shows the crack path in sample No. 1. It shows this sample has fiber bridging but the non-flat fracture surface is the dominant reason for a rising R-curve. In other words, R-curve in this sample have been miscalculated and fracture energy is less than what R-curve shows after 15 mm of crack growth.

Sample No. 3 also had density of 0.23 gr/cm$^3$ before infusion but the density after infusion was 0.27gr/cm$^3$ (higher than No. 1). The R-curve for this sample starts from 160 J/cm$^3$ and it shows some plateau behavior without considerable fiber bridging. After the crack propagates 35 mm length, the R-curve starts to go up. But the dominant reason for that is a non-flat fracture surface as can be seen in figure 6.13 for this sample. The fracture surface after 35mm crack growth is higher than what has been calculated. So, fracture energy did not get higher and raise in R-curve is because of miscalculation of fracture surface area.

For sample No. 2 the density was 0.28 gr/cm$^3$ and 0.33 gr/cm$^3$ before and after impregnation, respectively. The R-curve for this sample started from 135 J/m$^2$ (the same as regular Balsa in TL direction) and it goes up to 200 J/m$^2$ by crack propagation. It shows fiber bridging during propagation and also the fracture

surface for sample No. 2 , as shown in figure 6.14, is almost flat and it has rougher surface than sample No. 1 and No. 3, which shows more fiber bridging in this sample. Figure 6.15 is the crack path for sample No. 2 in TL direction and it also shows fiber bridging during crack propagation.

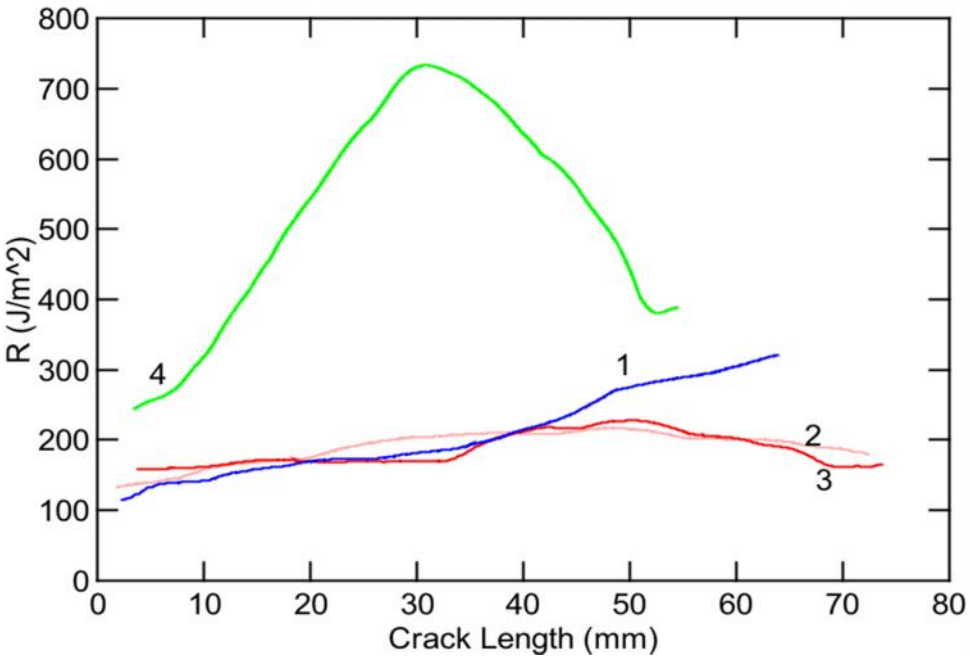


Figure 5.10. R-curve for different infused Balsa samples in TL direction.

Figure 5.11. Fracture surface for infused TL No.1.

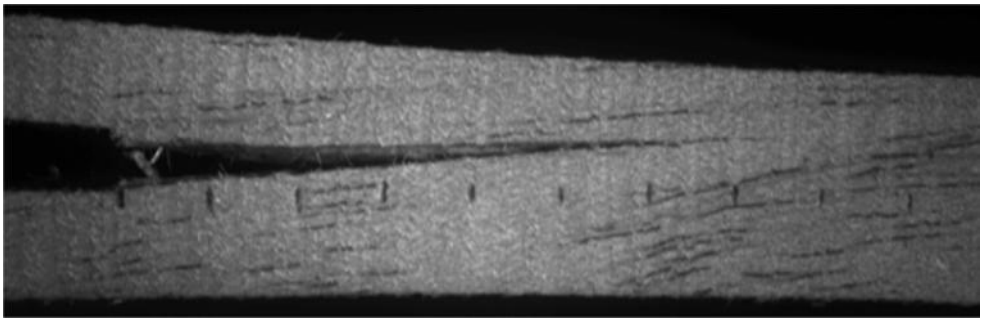

Figure 5.12. Crack path for infused TL1 sample.

Figure 5.13. Fracture surface for infused TL No.3 sample

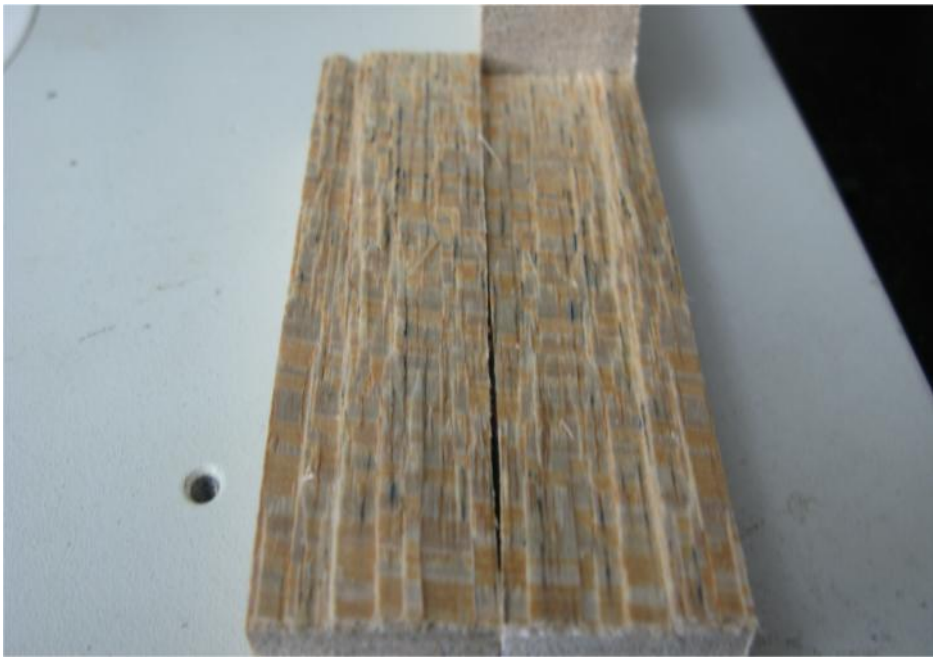

Figure 5.14. Fracture surface for infused TL No.2 sample.

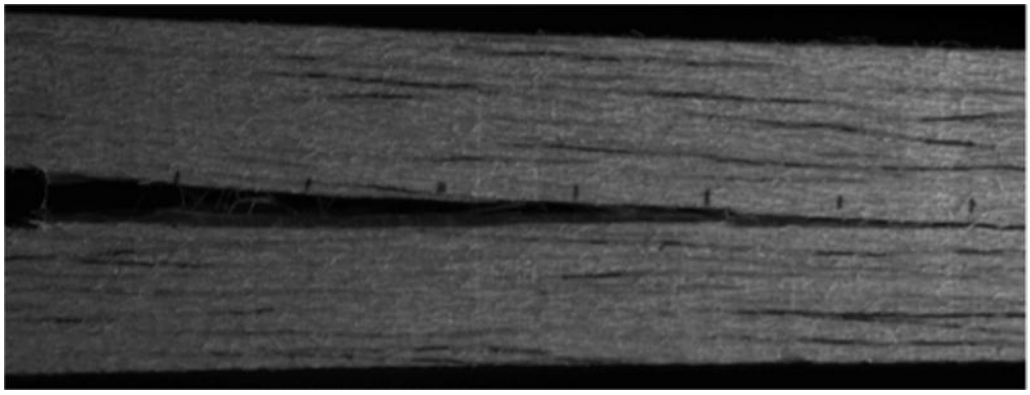

Figure 5.15. Crack path for sample No.2 infused TL.

Density of sample No. 4 was 0.37 gr/cm$^3$ and 0.44 gr/cm$^3$ before and after impregnation, respectively. The R-curve started from 240 J/m$^2$ and it goes up to 700 J/m$^2$ when crack reaches 30 mm. This shows considerable fiber bridging in this sample during crack propagation. As figure 6.16 shows fracture surface is also rough for this sample and it is almost jagged flat surface, which is result of fiber bridging. Also figure 6.17 shows the crack path for this sample and it has considerable fiber bridging. After crack reached 30 mm fracture energy came down. The fracture surface does not show any change after 30 mm crack grows in this sample. So, the only reason could be that the resin concentration is lower in that area around fracture surface that caused R-curve to drop. Another reason that after 30 mm crack growth fracture energy of this sample dropped is that crack was growing faster in area with lower fracture energy.

All in all the results for infused balsa in TL direction showed, when infused resin increases in Balsa wood, fracture energy tends to increase. But fiber bridging also depends upon the density of the raw Balsa. When density of Balsa is low, sample No. 1 and No. 3, resin infusion does not cause considerable fiber bridging during crack propagation but as the density of raw Balsa gets higher, then more infused resin caused more fiber bridging. For instance, in sample No. 4 the density of raw balsa was higher than others (0.37gr/cm$^3$) and the average of infused resin is 0.07 gr/cm$^3$ in the block and shows more fiber bridging than other samples in the TL direction. But, in sample No. 1 and No. 3 the density before infusion is low (0.23 gr/cm$^3$) and

infused resin does not have considerable effect on fiber bridging and it just increases starting point for R-curve (sample No. 3 had more infused resin and had more fracture energy also).

In general fracture surface of infused samples were rougher (and usually non-flat) than solid Balsa. This happens because of non-uniformity in resin infusion. So, crack goes through weaker area (lower resin impregnated area) and facture surface gets non-flat (raw balsa had mostly plateau fracture surface).

Figure 5.16. Fracture surface of infused TL No.4.

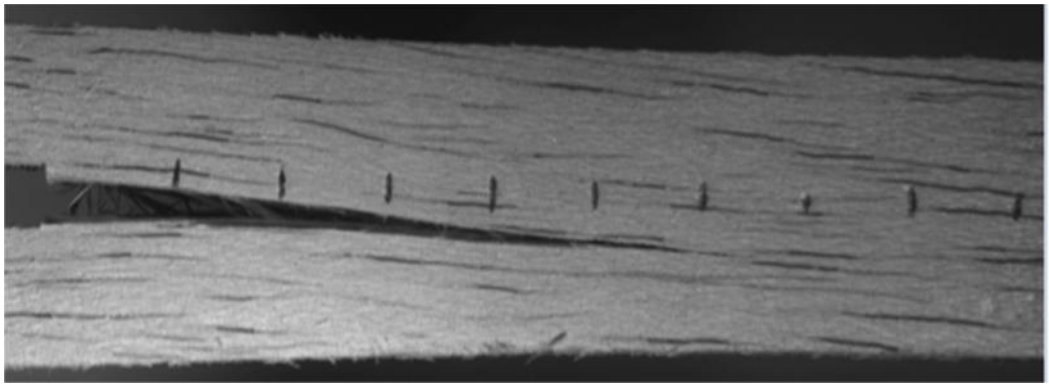

Figure 5.17. Crack path for infused TL No.4 sample.

# Chapter 6. Mode I fracture toughness of Banova samples

## *6.1. Introduction*

Banova is a commercial name for Laminated Veneer Lumber (LVL) made from Balsa wood. LVL is an engineered wood product that uses multiple layers of thin wood (typically 2-3 mm thickness for each layer) assembled with adhesives (Fig. 6.1). It offers several advantages over typical milled lumber: it is usually stronger, straighter, and more uniform and because it is manufactured from veneers, LVL makes up to 35% more effective use of logs than is possible with solid lumber. It is much less likely than conventional lumber to warp, twist, bow, or shrink due to its composite nature. Made in a factory under controlled specifications, LVL products allow users to reduce the onsite labor. They are typically used for headers, beams, rim board, and edge-forming material. Veneers are made by rotatory cutting of logs parallel to the growth ring, which is cheaper method, and it gives more uniform veneers (see Fig 6.2).

Figure 6.1 Banova (Balsa LVL) sample.

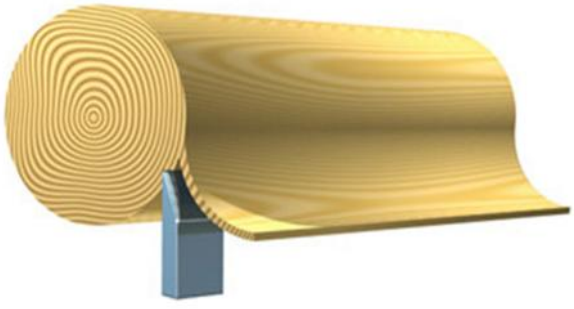

Figure 6.2. Rotatory cut for making veneer sheet.

Four different types of Banova samples were tested; G39 (infused and non-infused) and C31 (infused and non-infused). The difference between G39 and C31 is the adhesive used to glue the Balsa veneers. The adhesives were Polyurethane (PUR) for G39 Samples and Urea-formaldehyde (UF) for G31 samples. The difference between infused and non infused are specimens subjected to bonding process used to make sandwich composites without actually bonding the face sheets. In other words, the infused Banova specimens have been infused with the sandwich composite bonding resin. Balsa veneers were by rotary method. So, delamination of Banova during crack propagation is like fracture in RL direction (crack parallel to the glue line and along wood fiber directions) and TL direction is crack propagation normal to the glue line and parallel to the wood fibers direction (see Fig. 6.3).

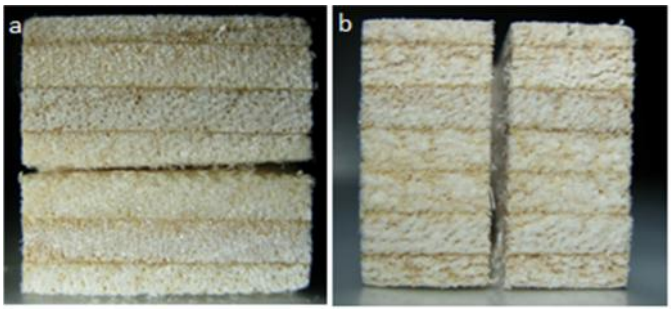


Figure 6.3. (a) Crack in RL direction (b) TL direction for Banova samples.

*6.2. RL G39*

Figure 6.4 shows R-curves for G39 samples in the RL direction (both infused and non-infused). For infused RL, the R-curve starts from 150 J/m$^2$ and goes up to 300 J/m$^2$ when the crack reaches 90mm. The fiber bridging in this sample is considerable and Fig. 6.5 shows crack path in this sample, which shows crack does not deviate from the mid-plane and fiber bridging is also obvious in crack path.

For sample RL 1, which was non-infused, the R-curve starts from 300 J/m$^2$ and during crack propagation go up to 450 J/m$^2$ after about 80 mm of crack growth. Figures 6.6 and 6.7 are fracture surface and crack path for this sample. The fiber bridging was clearly seen in the crack path and broken fibers on the rough fracture surfaces show fiber bridging in this sample.

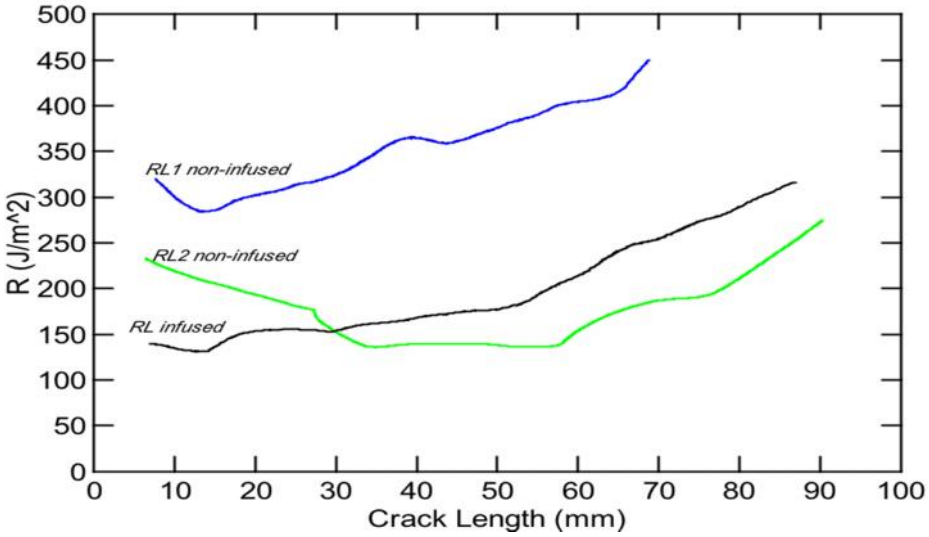


Figure 6.4. R-curve in RL direction for G39 samples.

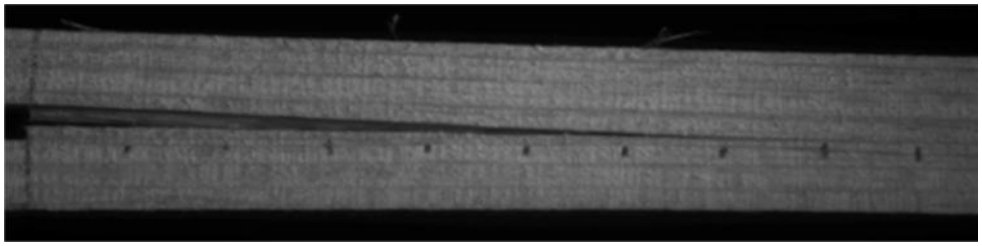

Figure 6.5. Crack path for G39 infused RL.

The initial, pre-crack for the RL 1 non-infused sample was in the middle on the central Balsa veneer (veneer Balsa was neutral plane) and not at a bond line. For sample RL2 (non-infused), the pre-crack was cut on a glue line (in this sample glue line was at the specimen's neutral plane). As figure 6.8 shows crack started next to the glue line in the veneer and later moved into the veneer layer (*i.e.*, the crack did not propagate completely on a glue line). The R-curve for this sample started around 250 J/m$^2$ and decreased gradually to 150 J/m$^2$ and then increased after reaching 60 mm or crack growth. The reason for the decreasing in fracture energy may be the notch started on a glue line, which had higher fracture energy. But, soon after initiation, the crack path can involve a weaker layer (the Balsa veneer in this sample). Later, the R-curve starts to rise because of fiber bridging. As shown in figure 6.9 during crack propagation, in first 20 mm fiber bridging is not considerable

because it is next to glue line. After that phase, more fiber bridging occurs when crack goes through veneer layer. Fiber bridging shows its effect after 60 mm crack grows in this sample; the fracture surface is then mostly in the Balsa veneer and it causes the increase in the R-curve for this sample. Figure 6.9 shows crack path for this sample and it shows more evidence of fiber bridging when the crack goes into the Balsa veneer. Figure 6,10 shows the fracture surface. It shows fracture surface is not completely flat which caused an increase in R-curve. In other words, although fiber bridging causes R-curve go higher, non-flat fracture surface can have that effect as well.

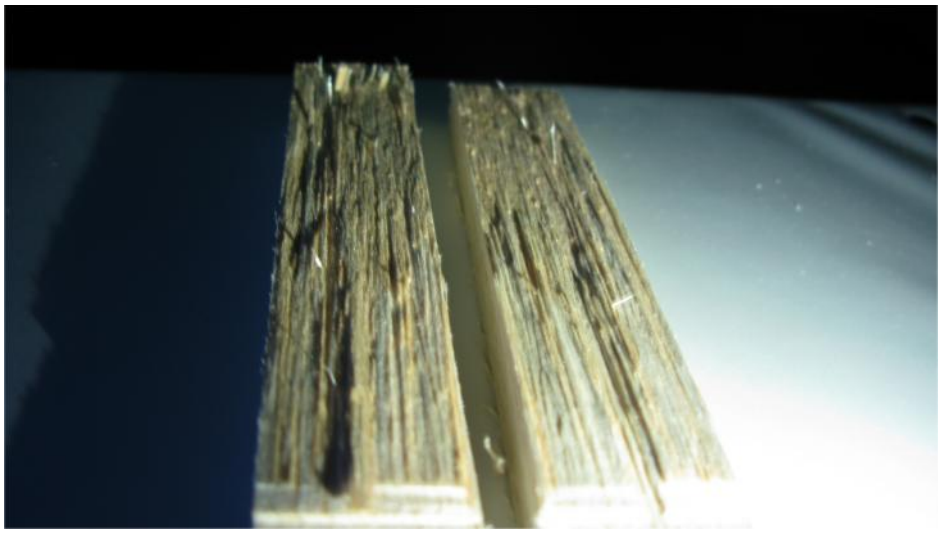

Figure 6.6. Fracture surface of G39 non-infused RL1.

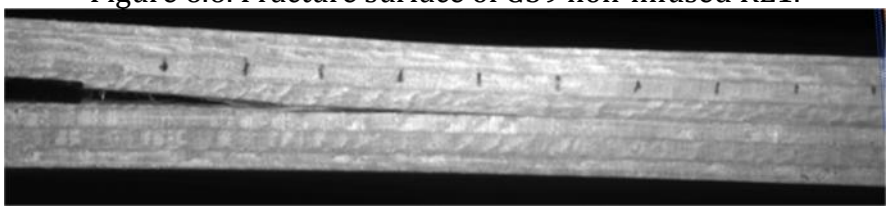

Figure 6.7. Crack path of G39 non-infused RL1.

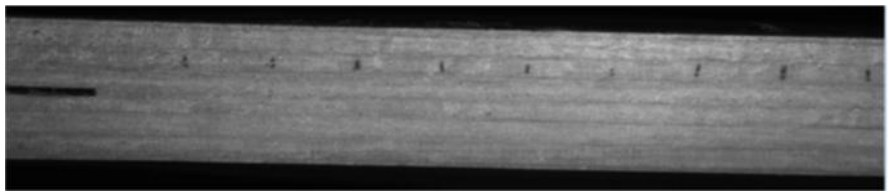

Figure 6.8. Pre-crack on glue line for G39 non-infused RL2 sample.

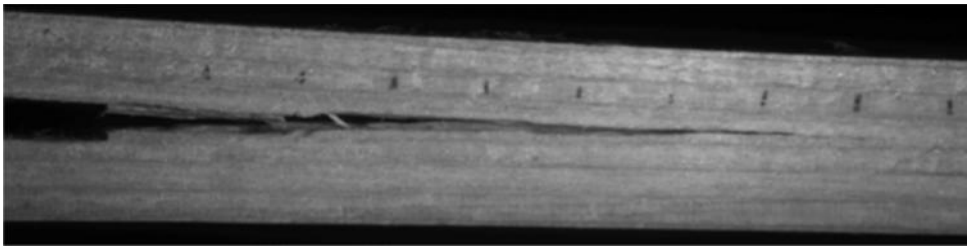

Figure 6.9. Crack path for non-infused RL2 from G39 samples.

*6.3. RL C31*

Figure 6.11 shows R-curves for C31 (infused and non-infused) samples in the RL direction. In non-infused sample (regular sample) R-curve starts from 80 J/m$^2$ and by crack propagation increases as result of fiber bridging. The slope of the R-curve changes after the crack reaches 40 mm and shows more fiber bridging behavior during crack propagation. The R-curve shows an approximate plateau behavior around 210 J/m$^2$ after crack growth exceeds 60 mm. The crack path for this sample is shown in figure 6.12 in which fiber bridging is observable.

Figure 6.10. Fracture surface for non-infused RL2 from G39 samples.

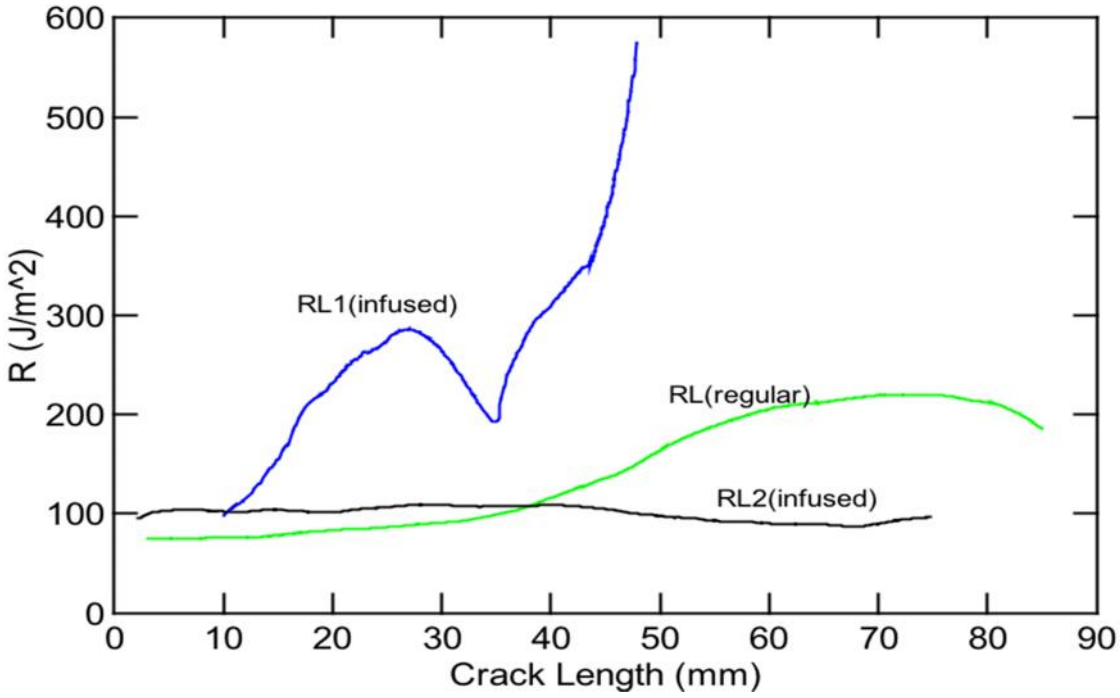


Figure 6.11. R-curves for C31 samples in RL direction.

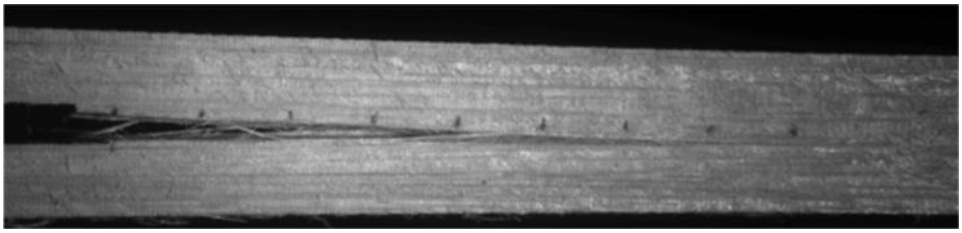

Figure 6.12. Crack path for non-infused RL from C31 samples.

For C31 infused samples, the results in the RL direction had two different results. Sample RL 2 infused shows a completely flat R-curve without fiber bridging around 100 J/m$^2$. As figure 6.13 also shows, this sample did not show fiber bridging during crack propagation and is probably clean fracture within a single Balsa veneer layer. In sample RL1 infused, the R-curve also starts from 100 J/m$^2$ but it shows considerable fiber bridging during crack propagation and the R-curve increases to 600 J/m$^2$ after 50 mm or crack growth. After that growth, the crack became unstable and the sample broke. Figure 6.14 also shows fiber bridging during crack propagation for this sample. Fracture surface of these two samples are shown in Fig. 6.15 and Fig. 6.16; the surfaces show that RL 2 infused has soft flat fracture surface

but RL 1 infused has jagged surface as a result of more fiber bridging during crack propagation. The surfaces explain the differences in the R curves.

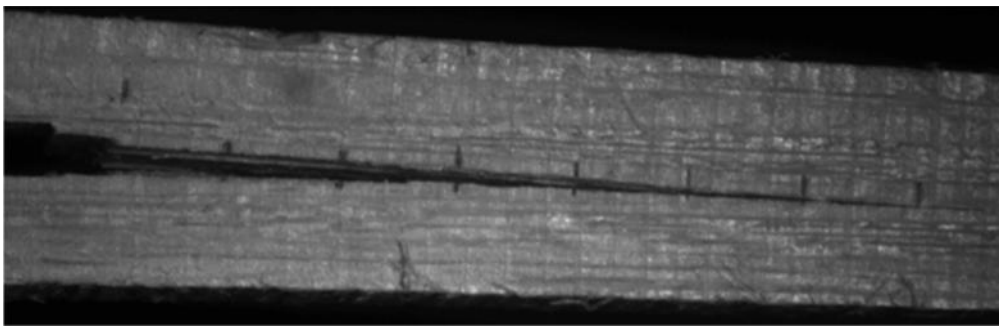

Figure 6.13. Crack path for C31 infused RL2 sample.

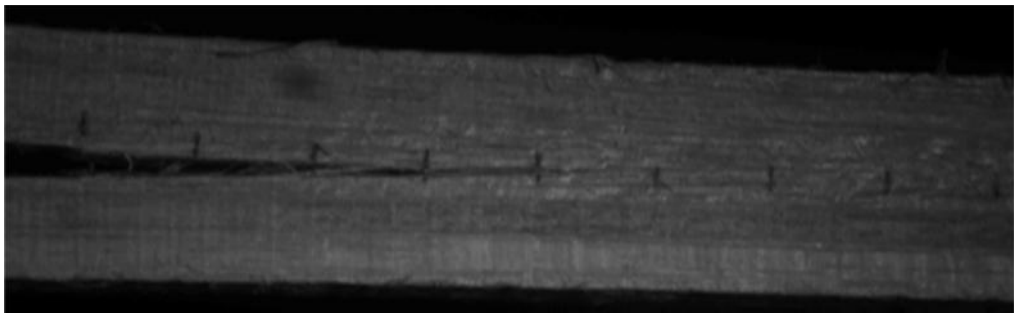

Figure 6.14. Crack propagation in C31 infused RL1 sample.

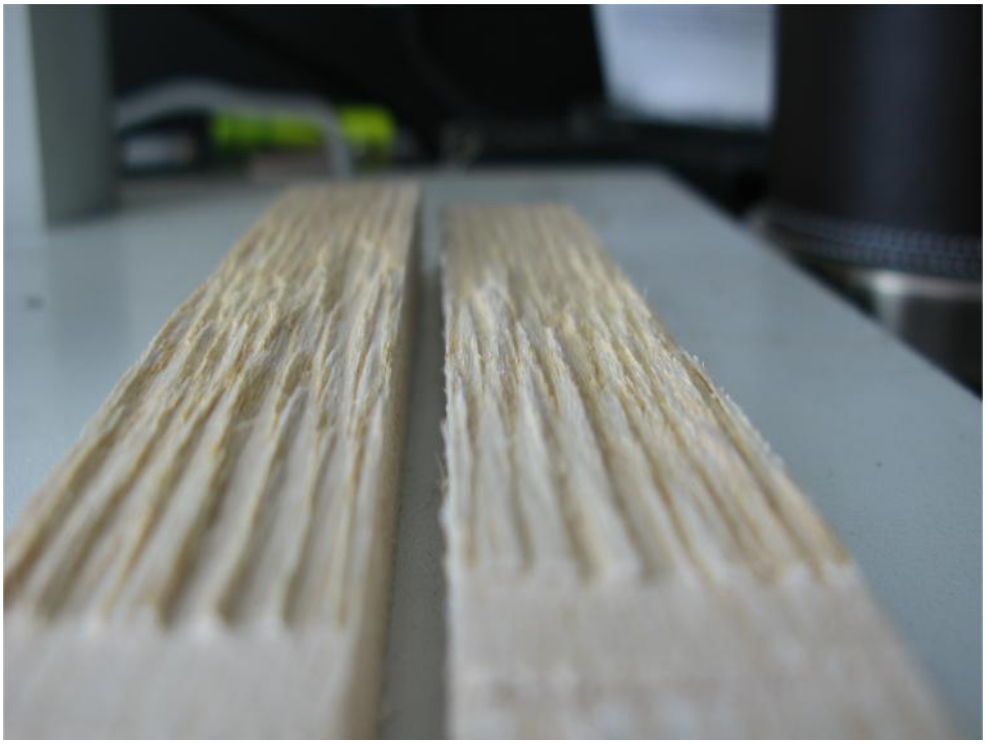

Figure 6.15. Fracture surface of C31 infused RL1.

Figure 6.16. Fracture surface of C31 infused RL2.

Microscopic pictures from fracture surfaces in figure 6.17 show both samples have infused resin in the veneer and so the only reason for this difference in fracture energy could be that these two veneers (fractured surface in these two samples) are from different Balsa wood or have different density. Figure 6.18 shows microscopic pictures from the side of the samples. In sample RL 1 infused wood fibers can be observed crossing the crack but in RL 2 fibers are aligned in crack direction and do not cross the crack, which suggests veneers had been chosen from different kinds of Balsa wood.

In summary, results showed that C31 samples in RL direction, non-infused samples does not have considerable difference in fracture energy, compared with high density Balsa wood in the RL direction, but infused C31 has around 25% higher fracture energy than high density Balsa wood. In contrast, the G39 samples were clearly tougher than both C31 samples and solid Balsa. The G39 infused samples had more than 100% increase in fracture energy and they showed clearly more fiber bridging than regular Balsa in the RL direction. Non-infused G39 Banova had higher fracture energy in RL direction than infused G39 and fracture energy was 200-300% higher than raw Balsa in this direction. It should be mentioned that infused G39 showed higher fiber bridging during crack propagation.

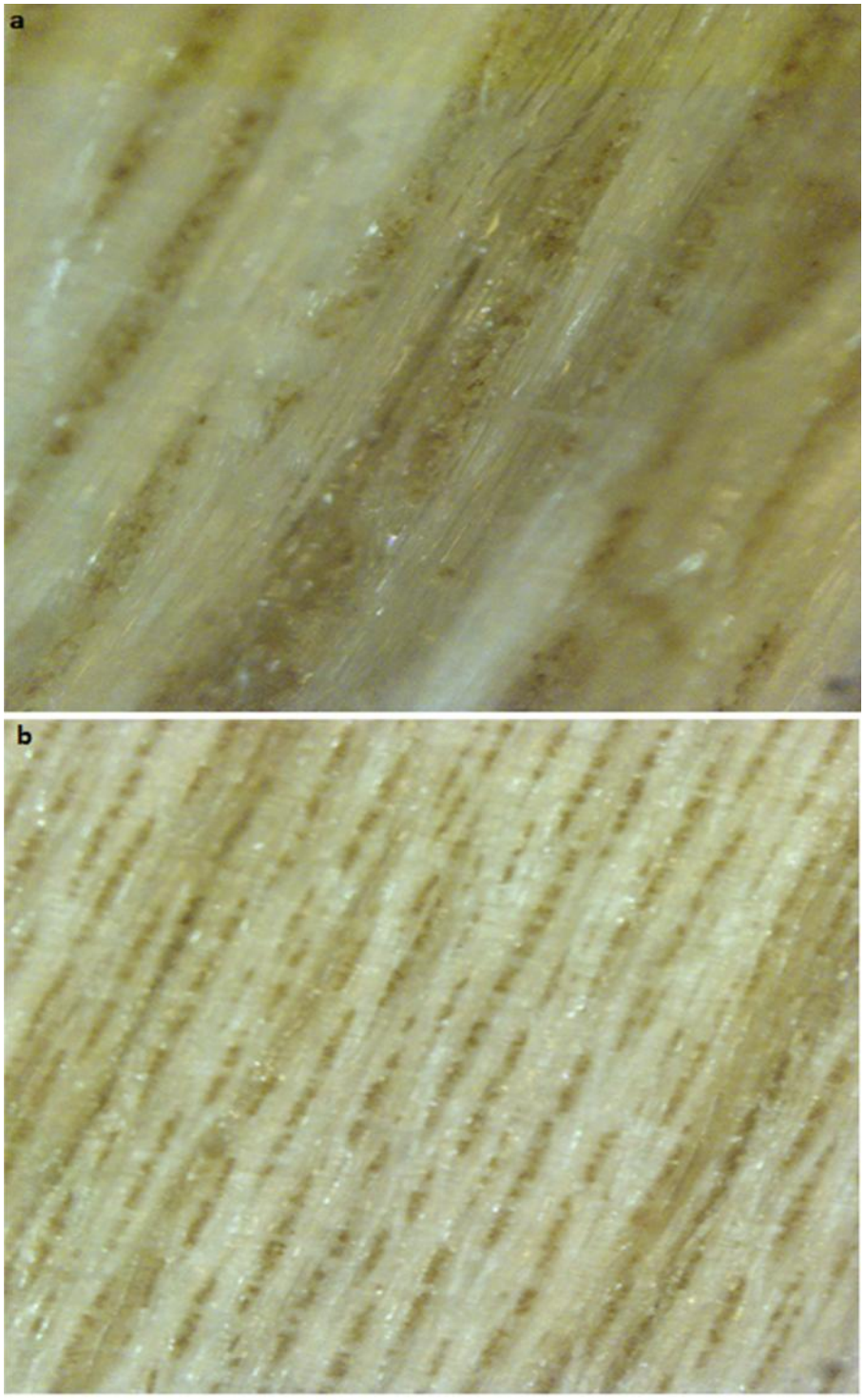


Figure 6.14. Microscopic photo from fracture surface for (a) C31 infused RL1 (b) C31 infused RL2 (55X magnitude).

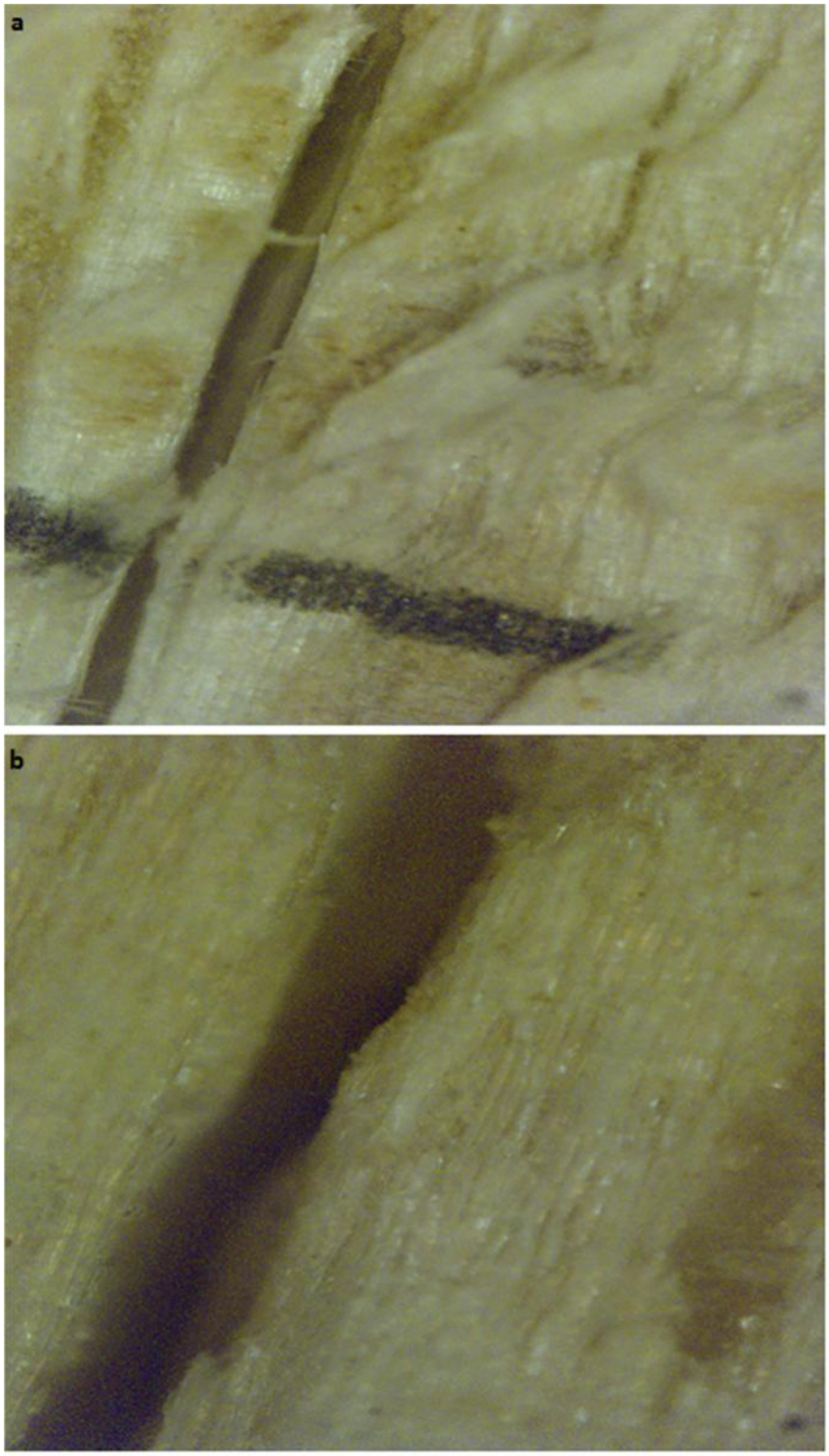


Figure 6.18. Microscopic photo from side of sample for (a) C31 infused RL1 (b) C31 infused RL2 (55X magnitude).

*6.4. TL G39*

Four G39 samples in TL direction were tested (two infused and two non-infused). Figure 6.19 shows consistent R-curves for all of four samples in this direction. For non-infused TL2 sample, the R-curve starts around 160 J/m$^2$ and goes up to 350 J/m$^2$ as result of fiber bridging when crack propagates about 40 mm and then drops after 60 mm, which could be result of non-uniformity in this sample. In the non-infused TL 1 sample, the crack starts to propagate when energy reaches around 250 J/m$^2$ and R-curve rises up to 350 J/m$^2$ when crack gets 40 mm and then shows a plateau behavior around 350 J/m$^2$. In infused samples, the R-curve for TL 1 starts from 170 J/m$^2$ and goes up to 400 J/m$^2$ when crack length gets around 40 mm and after that fracture energy becomes constant around 400 J/m$^2$. For TL 2 infused, the R-curve starts from 250 J/m$^2$ and increases up to around 550 J/m$^2$ when crack grows about 70 mm.

As the results showed, infused and non-infused G39 samples had little differences in TL direction and as it is obvious TL 1 infused and non-infused samples have almost the same R-curve and TL 2 infused and non-infused also showed almost the same R-curve. In other words, G39 infused and non-infused have almost the same fracture energy in the TL direction and the only difference is that when crack gets long. For toughness beyond 50 mm, the infused samples show higher fracture energy (more fiber bridging).

*6.5. TL C31*

The results for three C31 samples in the TL direction are discussed next. The R-curves for these samples are given in figure 6.20 For the non-infused samples in the TL direction, the R-curve started around 140 J/m$^2$ (like Balsa wood in TL direction) and it does not show considerable fiber bridging before 10 mm crack growth and then R-curve starts to increase up to 250 J/m$^2$ when crack length gets 30 mm and then comes done to around 150 J/m$^2$ when crack length become 40 mm. In other words, between 20mm to 40 mm crack length sample has a peak in fracture energy. The fracture surface shows before 20 mm and after 40 cm crack growth there are

some holes in glue lines and it shows the glue lines may help to increase fracture energy in that area where there is no defect on glue line and in all other places the fracture energy is the same as Balsa wood in the TL direction. Figure 6.21 shows the fracture surface for this sample.

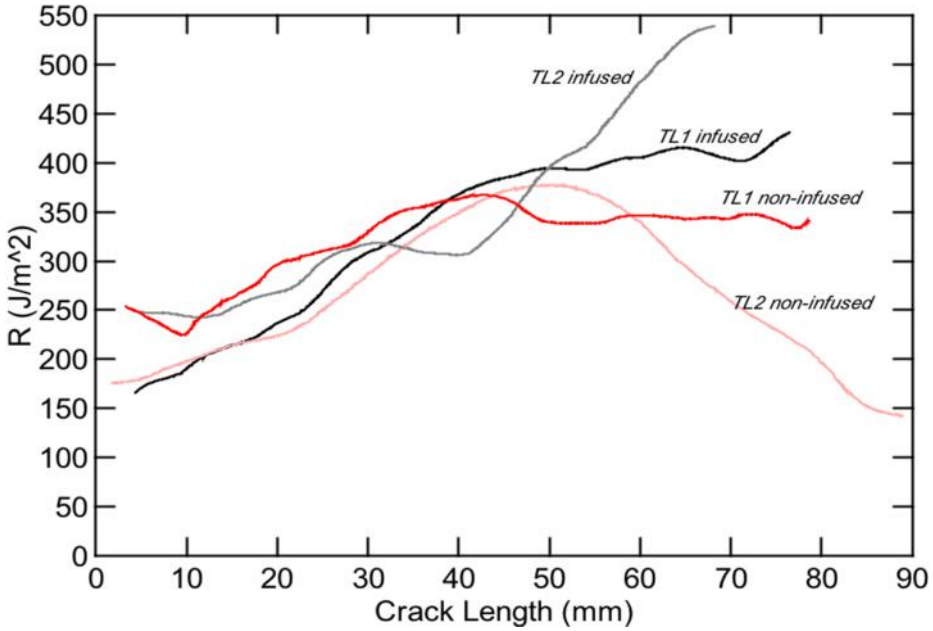


Figure 6.19. R-curves for G39 samples in TL direction.

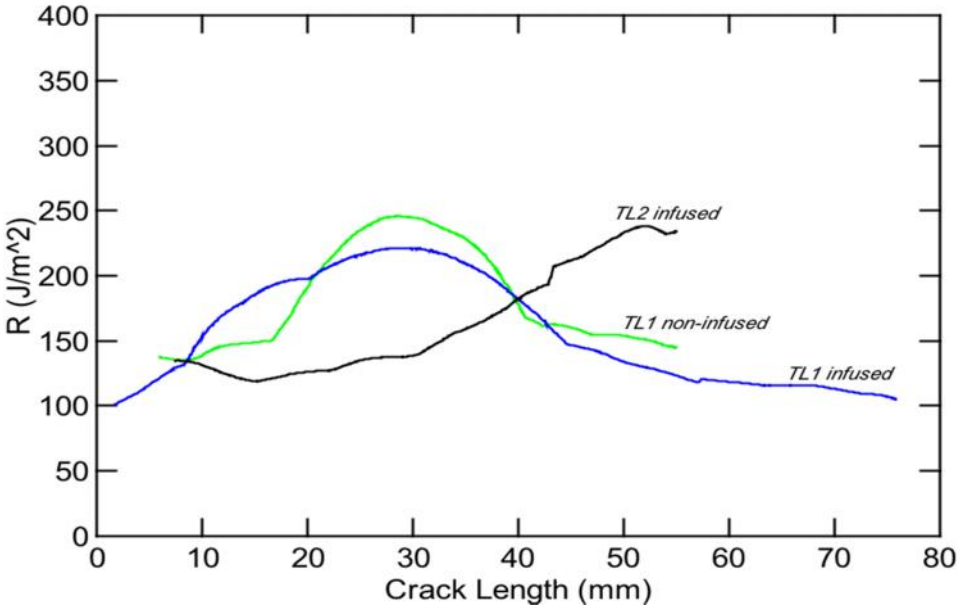


Figure 6.20. R-curves for C31 samples in TL direction.

Figure 6.21. Fracture surface of C31 non-infused TL sample.

The R-curve for TL 1 infused sample started from 100 J/m$^2$ and it rose up to 210 J/m$^2$ between 10-50 mm crack length and goes down to around 100 J/m$^2$ again. The fracture surface for this sample shows some layers have fiber bridging (not all of the layers) and that causes the increase in fracture energy. Also fracture surface is not flat in this sample, which caused to calculated fracture energy to be higher than what actual toughness. Therefore, in this sample fracture energy was lower than regular Balsa wood. Figure 6.22 shows the fracture surface for this sample.

For sample TL 2 infused, the R-curve started around 120 J/m$^2$ and by crack propagation goes up to 250 J/m$^2$ and then breaks when crack reaches around 55 mm length. This sample shows fiber bridging more than other C31 samples in the TL direction. But, it should be mentioned that figure 6.23 shows fracture surface is not flat and it is higher than what has been assumed for fracture energy calculation. So, fracture energy for this sample is lower than what the R-curve shows.

All in all, the results for Banova samples showed for C31 samples in TL direction, infusion not only does not help to increase fracture toughness, but also decreases starting point in comparison with regular Balsa wood in the TL direction. Non-infused C31 showed almost the same fracture toughness as regular Balsa in the TL direction. In the RL direction for C31 samples, non-infused samples showed almost the same fracture toughness as high density Balsa wood in RL direction (sample RL3 in chapter 3). Infused C31 showed less than 20% increase in fracture toughness

without fiber bridging which causes fracture toughness of infused C31 to become lower than regular balsa when the crack gets longer (picture for sample TL 2 infused C31 shows the fracture is not in pure RL direction and fibers crossed the crack which caused increase in toughness).

For G39 samples in the TL direction both infused and non-infused have almost the same fracture toughness and the only difference was that the infused samples showed more fiber bridging when crack gets long (in these samples, when it was more than 50 mm of growth). In both infused and non-infused samples, the fracture toughness is higher than regular Balsa wood (20-80% higher). They also showed considerable fiber bridging in the TL direction but in regular Balsa the bridging was negligible. In the RL direction non-infused samples showed higher fracture toughness than infused samples (G39) and when crack propagates infused sample might have lower or higher R-curve than non-infused (depends on if the crack is on a glue line or inside a veneer). Both the non-infused and infused G39 samples have higher fracture toughness (100-400% higher) than regular Balsa in the RL direction and fiber bridging is also higher than regular Balsa in this direction.

Figure 6.22. Fracture surface of C31 infused TL1.

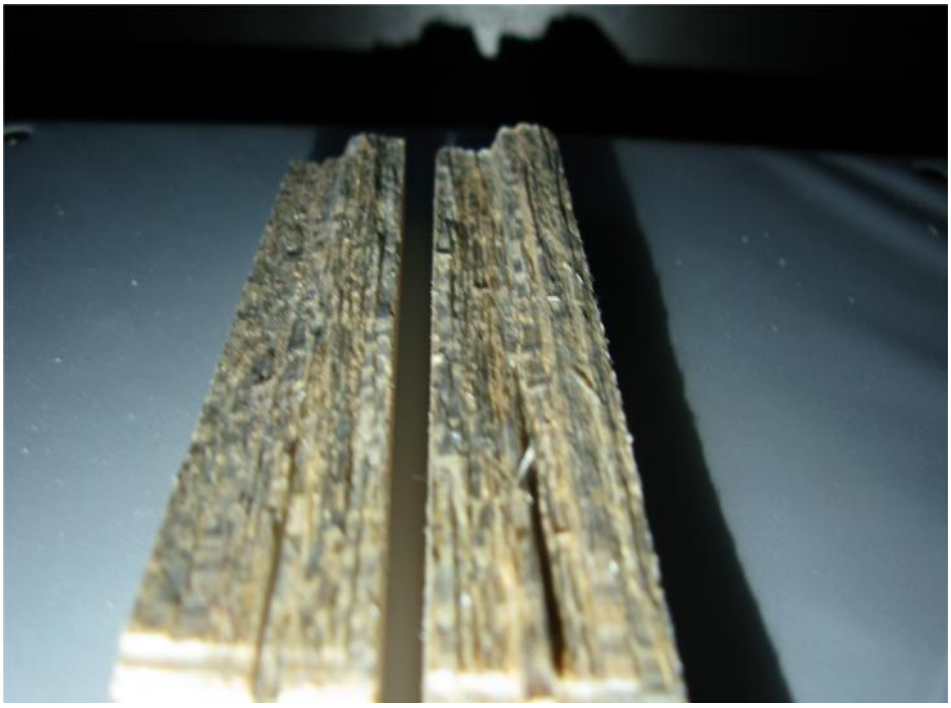

Figure 6.23. Fracture surface for C31 infused TL2 sample.

# Chapter 7. Balsa sandwich composite

## *7.1. Introduction*

Balsa, a highly processed ultra light wood product, imparts impressive strength and stiffness to the sandwich panel. The end grain configuration of balsa provides high resistance to crushing, and is very difficult to tear apart. End grain balsa cored panels also have the ability to handle excessive dynamic loads. Until recently, end grain balsa was excluded from some weight sensitive applications, as there were lower density foam cores available. Now, through controlled growing and careful selection, balsa wood is competitive in weight, as well as offering superior performance in stiffness and strength, particularly where local crushing or bruising is a concern. Most significant concern for these panels is fracture failure during load. Fracture might occur in the core (raw balsa, infused Balsa or Banova) or at the bond between the core and the skin. In previous chapters fracture properties of core

materials was discussed. This chapter focuses on fracture energy of skin/core adhesive bond.

*7.2. Materials and Methods*

To investigate fracture energy for bonding of the skin to Balsa in a sandwich composite, a three-point bending test was used. Figure 7.1 shows a schematic picture of the samples. The skins were two layers of pre-preg fiber glass/ epoxy at the top and bottom. The thickness of the skins was 1.8 mm and Young's modulus in long direction was 46 GPa (reported by supplier). The core was balsa wood with average density of 0.32 gr/cm$^3$ cut such that the wood fibers were perpendicular to the skin. The thickness of the core was 40 mm and Young's modulus along the axis of the beam, which is in the transverse direction of the wood, was 200 MPa (reported by supplier). The specimens were 100 mm wide and 200 mm long. The top skin was longer, by about 40 mm, with a 10 mm pre crack in the bonded part between skin and core, which was made during manufacturing by using Teflon to prevent bonding between the core and skin. All samples were prepared by 3A Composites company.

After data collection, fracture energy was calculated by using two different methods; theoretical energy release rate equation, John A. Nairn 2006, and also finite element analysis (FEA).

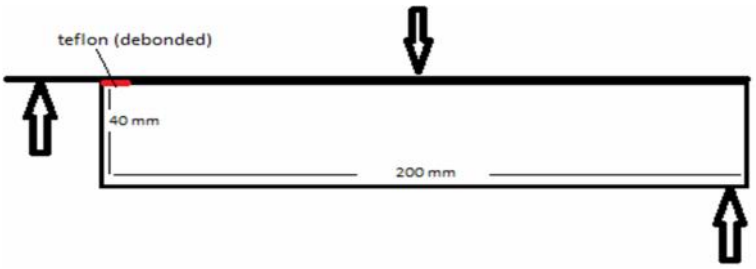


Figure 7.1. Schematic picture of the sandwich composite samples

*7.3. Fracture toughness of bonded part in Sandwich composite*

In order to find fracture energy for bonding, the assumption was the residual stresses could be ignored. Therefore, after eliminating these terms, Nairn 2006, equation 7.1 is used to find fracture energy. As shown in Eq. 7.1, P is force, a is

distance between support point and crack tip, $\varsigma_{\kappa}^{(1)}$ and $\varsigma_{\kappa}^{(3)}$ are compliances for curvature of the left skin and the right three-layered beam, respectively, B is width of the sample, $t_1$ and $t_2$ are thickness of skin (1.8mm) and core (40mm), $E_1$ and $E_2$ are Young's modulus for skin and core along the long axis of the beam [11].

$$G = \frac{P^2\, a^2}{8B}\left(\varsigma_{\kappa}^{(1)} - \varsigma_{\kappa}^{(3)}\right) \quad Equation\ 7.1$$

$$\varsigma_{\kappa}^{(3)} = \frac{12}{BE_1 t_1^3}\frac{R\lambda^3}{1-6R\lambda+12R\lambda^2+8R\lambda^3} \qquad \varsigma_{\kappa}^{(1)} = \frac{12}{BE_1 t_1^3} \qquad \lambda = \frac{t_1}{t_2} \qquad R = \frac{E_1}{E_2} \approx$$

230

After finding G for different crack lengths, the R curve as a function of crack length was plotted. Figure 7.2 shows five different R curves. As it is clear, for all of them R curve starts around 125 J/m$^2$ and goes up to 400-500 J/m$^2$ as the crack length increases. Figure 7.3 shows a process zone of fiber bridging during crack propagation, which causes the increase in fracture toughness of the bonded part. After about 55 mm of crack propagation, it was hard to continue the test because of large total deflection. So, after that the results are not reliable. The starting points for R curve in all samples are almost the same but as crack grows the R curves have some differences. One of the reasons for that could be the resin is not completely distributed the same in the entire surface and it can affect the fracture energy. Another possibility for this difference could be that the Young's modulus for balsa core and samples might not be the same and the average properties were used in these calculations. Another reason, which is more important, is that the crack propagation on bonded part was not completely stable. In other words, cracks were tracked from just one side and the assumption is crack grows at the same time stably across the width of the samples. But, during some tests, the crack on the front side, which was being tracked by camera, or backside, which was not tracked, went at different speeds. So, it caused the different apparent fracture energy rather than the actual differences in fracture toughness.

In order to test validity of our results by Eq. 7.1, Finite element analysis (FEA) was also used with different mesh size to see the effect of that and also mode mixity was

checked also by FEA using crack closure [12]. A regular mesh of elements was used, where the element size was the same as the thickness of skin (1.8 mm) and different forces (P) and crack size (a), which were gotten from experiment, were used to get fracture energy of bonding part by FEA. Figure 7.4 shows picture of FEA sample with mesh. A regular mesh was used because it was recently found to give more reliable results for crack closure mode mixity calculations [Nairn, personal communication].

The raw data were analyzed again by FEA. As figure 7.5 shows the finite element analysis predicts higher fracture toughness than theory. FEA results are 20-30% higher than theory. One reason could be the beam theory, which is used in analytical models. In other words, the thickness of the core makes the beam aspect ratio lower, which leads to inaccuracy in beam methods. The problem is magnified by the low shear modulus of the core relative to the skins, which causes shear deformation effects. In order to investigate the effect of thickness on analytical *vs*. FEA results, in one analysis, different core thicknesses were used and in other analysis different skin thicknesses.

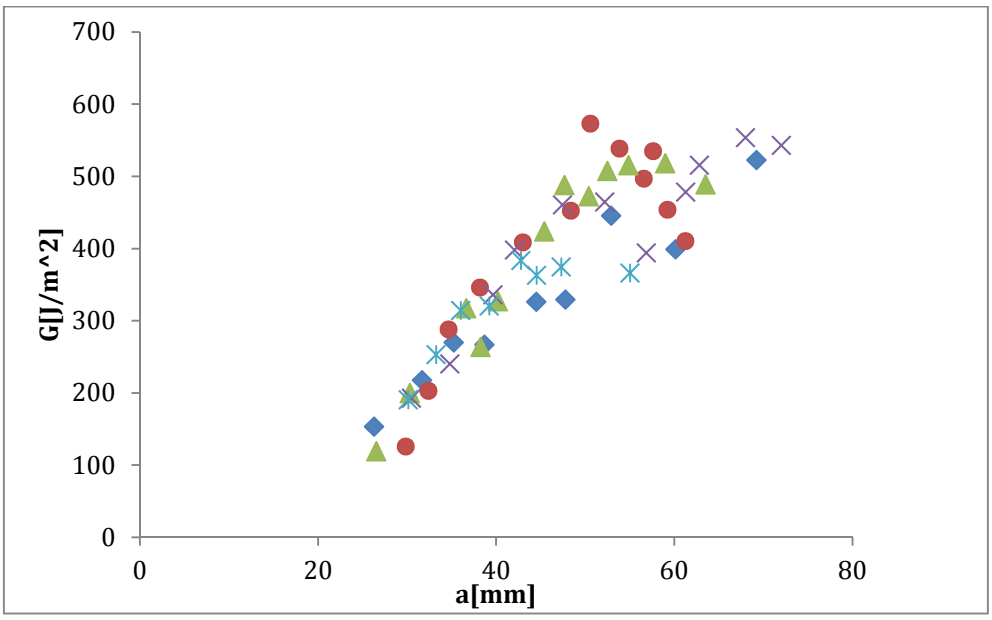


Figure 7.2. Fracture energy curve as function of crack length for all of 5 sandwich samples.

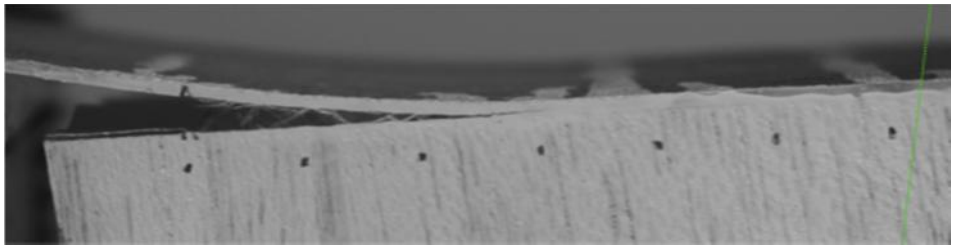

Figure 7.3. Process zone of fiber bridging in bonding part of sandwich panel.

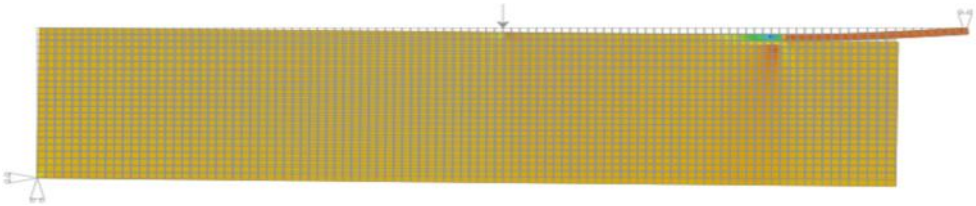

Figure 7.4. Picture of FEA sample with mesh.

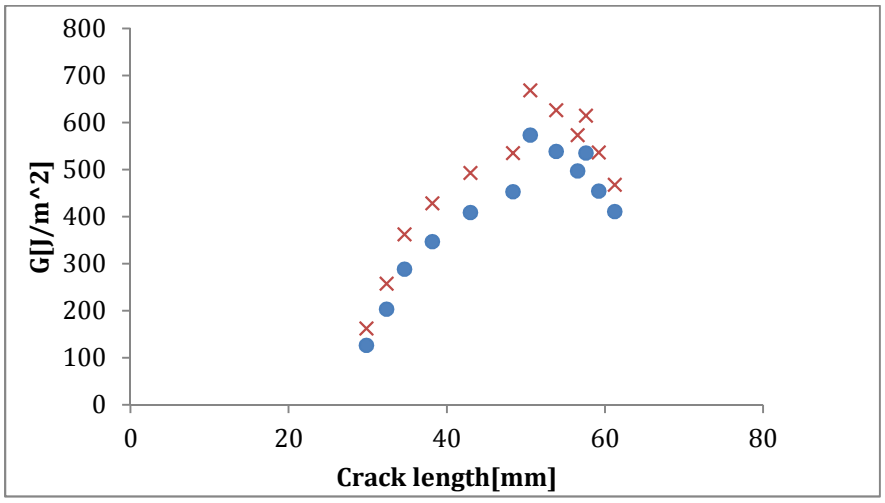


Figure 7.5. (Blue circles) R-curve from theoretical equation (red crosses) R-curve from FEA.

The core's thickness was varied over the range from 4 mm-40 mm. As Figure 7.6 shows the error between analytical model and FEA is almost constant for different thicknesses in core at about around 23%. This result shows any change in core's thickness does not affect the errors much.

The skin's thickness was varied from 1 mm to 3 mm in the FEA analysis. As figure 7.7 shows, by decreasing the thickness, the error decreases linearly (error was the difference between FEA results and theory). It was hard to reach the result for less than 1 mm thickness in FEA calculations; the error appears to extrapolate to very

low error when the skin is very thin. In conclusion, the difference between FEA and analytical model is probably inaccuracies in the beam theory caused by the large stiffness mismatch between the skin and the core and the errors get larger as the stiffness mismatch gets larger.

The effect of mesh size in FEA results for these tests also was also investigated. Three different mesh used uniform square elements with sizes of 0.6 mm, 0.9mm and 1.8 mm. the results showed the mesh size changed the fracture energy by less than 3%. In the other word, element size effects for this FEA analysis were negligible.

So far, all of the results for fracture toughness of bonded part in sandwich composite calculate the total fracture energy. Indeed, it is not clear whether these tests are mode I fracture or if they are dominated instead by mode II. In order study mode mixity effects, the crack closure methods in the FEA analysis were used to calculate this specimens loading conditions. The results showed, less than 0.3% of the total energy release rate is in mode II and therefore mode I dominated all these experiments. The specimens might be expected to produce more mode II, but apparently the large mismatch in stiffness between the core and the skin makes the mode II component negligible.

I suggest a brief summary the bonding toughness starts around 125 and increase due to fiber bridging, is mostly mode I, and is high the raw Balsa mode I. The interface is probably good enough for making sandwich core laminates.

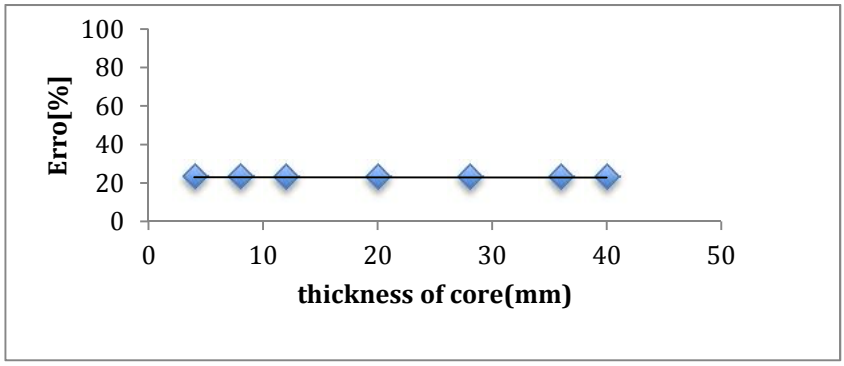


Figure 7.6. The error between analytical model and FEA. For different thickness of core.

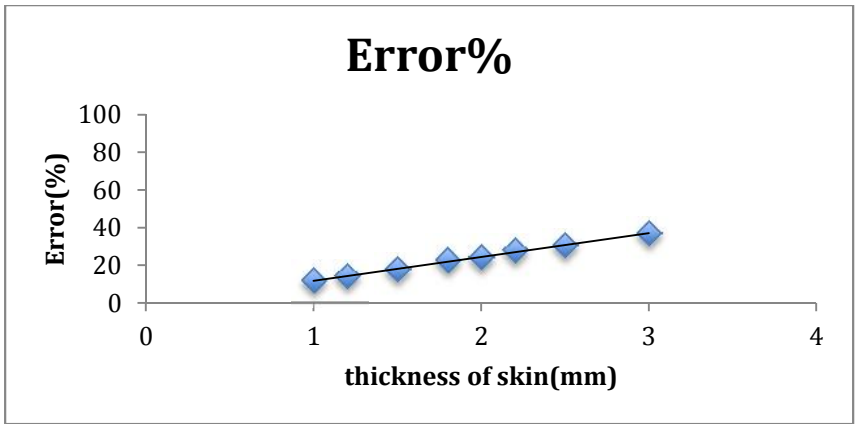


Figure 7.7. The error percentage decreases as thickness of skin reduces.

## Chapter8. Conclusion

1. Fracture properties of Balsa were fully characterized.
2. Mode I toughness in the TL direction is higher than RL direction and both have some effects of fiber bridging.
3. Mode I R-curve in TL direction for Balsa wood starts around 140 $J/m^2$ and it does not show considerable fiber bridging during crack propagation (less than 10 percent increase in Fracture energy when crack gets long) and R-curve is almost plateau.
4. . Density measurement for samples in TL direction showed that the density does not affect fracture energy of Balsa in TL direction.
5. Mode I R-curve in RL direction had different starting points depends on density of samples. It started around 50 $J/m^2$ for sample with 0.2 $gr/cm^3$ density and R-curve showed plateau behavior (see sample No.1 in Fig. 3. 1). But for sample with density of 0.34 $gr/cm^3$ R-curve started from 75 $J/m^2$ and goes up to 125 when crack propagates.
6. The density measurement for RL samples showed as density increases, Fracture energy will increase and samples with higher density show more fiber bridging during crack propagation.
7. In the transverse plane, crack tends to turn to the RT direction to remain within a single growth ring and probably within the lower toughness early

wood.

8. In RT direction Mode I fracture toughness was varied (from 80 $J/m^2$ to 400 $J/m^2$ starting point for R-curve) in specimens and tends to get higher when density of sample is higher.
9. The toughness is affected by density, but to a much smaller extent than predicted by Gibson and Ashby scaling. In RT direction this effect was higher than RL and TL directions (more fiber bridging).
10. Compared to other species (e.g., Douglas fir), the toughness is lower, but not as low as prior scaling models predict considering its much lower density. Overall, Balsa toughness is surprisingly high for such a low density material.
11. Mode II fracture toughness is much higher, independent of direction (TL vs. RL) and shows no influence of fiber bridging.
12. Mode I crack sometimes deviate (due to grain direction) and therefore become mixed mode. The results can be plotted on a GI/GII surface. Interpretation of the experiments is complicated by simultaneous development of fiber bridging during the crack propagation.
13. . Infusing on vinyl ester resin into the Balsa tends to increase toughness, but not by a large amount. The presence of resin, most likely non-uniformly distributed within the large pores, tends to lead to rougher (and non-flat) fracture surfaces. In the other word, because of non-uniform impregnation crack goes through the area with lower amount of resin.
14. . Laminating Balsa veneers into a Balsa LVL, known as Banova, has improved toughness compared to solid Balsa. The Banaova toughness depends on resin used to glue the veneers with PUR resin giving tougher specimens than UF resin. Like solid Balsa, Banova toughness with infused vinyl ester resin is not much different then non-infused Banova and the difference is that the infused benova shows more fiber bridging when crack gets long.
15. For use of Balsa in sandwich code composites, the interfacial toughness between the skin and the Balsa core can be found by a three point bend

specimen. Due to the large mismatch between skin and core properties, this fracture is close to a pure mode I toughness. The bond between glass fiber skin and Balsa core has a high toughness (higher than the solid Balsa) and therefore probably not a limiting feature for Balsa core sandwich composites.

## References:

[1]- K. E. Easterling et al., "on the mechanics of Balsa and other woods," *proc. R. soc. Lond..A.*, 1982; 383: pages. 31-34.

[2]- J. F. Dreisbach, Balsa wood and its properties, Colombia Graphs, 1952.

[3]- I. Smith et al., Fracture and Fatigue in wood, John Wiley & Sons, 2003.

[4]- D.F. Adams el al., "Experimental characterization of advanced composite materials; third edition,CRC Press,2002.

[5]-M. F. Ashby el al., "The fracture toughness of woods, " proc. R. soc. Lond..A, 1985; 398: 261-280.

[6]- G.Jeronimidis,, "the fracture behavior of wood and the relations between toughness and morphology'" Proc. Soc.Lond. B , 1980;208: 447-460.

[7]- Noah Matsumoto el al.,"The Fracture Toughness of Medium Density Fiberboard (MDF)," Engr. Fract. Mech.,2009;76,: 2748-2757.

[8]- J. A. Nairn, el al., "Fracture Modeling of Crack Propagation in Wood and Wood Composites," 12th International Conference on Fracture, Ottawa, Canada, 2009; July 12-17

[9]- Noah Matsumoto el al., "Fracture Toughness of Wood and Wood Composites During Crack Propagation," Wood and Fiber Science, 2012;44:121-133.

[10]- J.A. Nairn, "Analytical and Numerical Modeling of R Curves for Cracks with Bridging Zones," International Journal of Fracture, 2009; 5: 167-181.

[11]- J. A. Nairn., "On the Calculation of Energy Release Rates for Cracked Laminates with Residual Stresses," Int. J. Fracture, 2006;139: 267-293.

[12]- J.A. Nairn, "Generalized Crack Closure Analysis for Elements with Arbitrarily-Placed Side Nodes and Consistent Nodal Forces," Int. J. Fracture, 2011; 171: 11-22.

[13]- John A. Nairn, "Numerical Implementation of Imperfect Interfaces," Computational Materials Science, 2007; 40: 52.